

BUBBLE NUCLEATION
IN
SATURATED AND SUBCOOLED BOILING

BUBBLE NUCLEATION
IN
SATURATED AND SUBCOOLED BOILING

By
PABITRA LAL DE, B.TECH. HONS.

A Thesis
Submitted to the School of Graduate Studies
in Partial Fulfilment of the Requirements
for the Degree
Master of Engineering

McMaster University

April 1973

MASTER OF ENGINEERING
(Mechanical Engineering)

McMASTER UNIVERSITY
Hamilton, Ontario.

TITLE: Bubble Nucleation in Saturated and Subcooled
Boiling

AUTHOR: Pabitra Lal De, B.Tech. Hons.

(Indian Institute of Technology, Kharagpur)

SUPERVISOR: Professor Ross L. Judd

NUMBER OF PAGES: (viii), 90

SCOPE AND CONTENTS:

An experimental investigation is reported for water boiling at atmospheric pressure on a copper surface. Bubble nucleation at an artificial site was observed for five heat fluxes between 11,000 and 20,000 BTU/Hr Ft², and subcooling from 0° to about 30°F. Using Wiebe's correlation for heat flux and superheat layer thickness, four mathematical models were tested. The measured results are found to provide excellent agreement with the Han and Griffith model for bubble nucleation.

ACKNOWLEDGEMENTS

It is my pleasure to gratefully acknowledge the expert guidance and advice of Dr. R. L. Judd for suggestions in planning and performance of this experimental work.

I would like to express appreciation to Miss Erie Long for typing the manuscript.

The financial support provided by the National Research Council Grant A4362 is also acknowledged.

TABLE OF CONTENTS

CHAPTER		PAGE
I	INTRODUCTION	1
II	LITERATURE SURVEY	3
III	THEORETICAL CONSIDERATIONS	14
	3.1 Bankoff Model	15
	3.2 Griffith and Wallis Model	22
	3.3 Hsu Model	25
	3.4 Han and Griffith Model	34
IV	EXPERIMENTAL APPARATUS	38
	4.1 Design Criteria	38
	4.2 Test Assembly	39
	4.3 Heating System	41
	4.4 Injection System	41
	4.5 Cooling System	43
	4.6 Power and Controls	43
	4.7 Thermocouples	45
	4.8 Temperature Measuring System	46

TABLE OF CONTENTS - continued

CHAPTER		PAGE
V	TEST CONDITIONS	49
VI	TEST PROCEDURE	51
VII	RESULTS	54
VIII	DISCUSSION	65
IX	CONCLUSION	73
APPENDIX		
A	EXPERIMENTAL DATA AND CALCULATIONS	74
B	HEAT LOSS CALCULATION	79
C	UNCERTAINTY ANALYSIS	83
REFERENCES		87
NOMENCLATURE		89

LIST OF FIGURES

FIGURE		PAGE
1	Griffith and Wallis' data	6
2	Effect of subcooling and pressure on incipient boiling	9
3	Incipience of boiling data	12
4	Model for liquid penetration (Bankoff)	16
5	Nucleation at conical cavity with 90° contact angle	23
6	Bubble nucleus at cavity mouth	27
7	Model for temperature profiles (Hsu)	27
8	Temperature profile $\xi(\eta, \tau)$ for constant surface temperature	31
9	Activation of cavities	31
10	Temperature distribution near a heating surface	36
11	Sectional view of test assembly	40
12	Electrical connections diagram	42
13	Copper heating surface	44
14	Thermocouple circuit connections	47
15	Heat flux - superheat characteristics	55

LIST OF FIGURES - continued

FIGURE		PAGE
16	Variation of wall superheat with bulk subcooling	56
17	Superheat layer thickness correlation (Wiebe)	66
18	$\theta_{w_E}^*$ versus $\theta_{w_P}^*$ (Griffith and Wallis)	68
19	$\theta_{w_E}^*$ versus $\theta_{w_P}^*$ (Hsu, $\phi = 53.2^\circ$)	69
20	$\theta_{w_E}^*$ versus $\theta_{w_P}^*$ (Hsu, $\phi = 70^\circ$)	70
21	$\theta_{w_E}^*$ versus $\theta_{w_P}^*$ (Han and Griffith)	71
22	Heat loss calculations	80

LIST OF TABLES

TABLE		PAGE
I	Range of subcooling for different heat fluxes	50
II	Experimental data $\theta_s, \theta_w, \theta_{w*}$	58
III	Experimental data and calculations h, δ and $\theta_{w_p}^*$	75

C H A P T E R I

INTRODUCTION

Nucleate boiling has been of considerable interest to heat transfer engineers because of the high heat transfer coefficients associated with the phenomenon. Yet, the problem of nucleate boiling remains far from being understood completely inasmuch as the data available from various sources do not agree with one another. The outstanding feature of nucleate boiling is that bubbles usually originate at specific locations on the heated surface. Numerous still photographs and electron micrographs of the surface have been taken, demonstrating that bubbles originate from microscopic pits and scratches on the surface.

As a result of this work, the importance of surface micro-structure on nucleate boiling has now been recognized and efforts are being made to investigate the distribution, size and shape of potentially active nucleation sites. However, the prediction of surface superheat/heat flux characteristics of a boiling surface is further complicated by a general lack of knowledge of the mechanism governing the nucleation of bubbles at active sites. It is this problem to which the thesis addresses itself. There are a number of theories explaining nucleation phenomenon in

relation to surface condition, but none gives a complete picture. The present work concentrates on bubble nucleation at an artificial nucleation site of known dimension and provides valuable information regarding the mechanism of bubble nucleation in saturated and subcooled boiling.

CHAPTER I I

LITERATURE SURVEY

Corty and Foust [1] studied the influence of surface microroughness and contact angle on nucleate boiling. They measured the heat transfer coefficients of ether, normal pentane, and Freon 113 from a horizontal heated surface. Measurements of the surface roughness were made using a Profilometer, and photo and electron micrographs of the surfaces were also taken.

Their experiments indicate that the shape and size distributions of the microroughness in the heat transfer surface are definite variables in determining the superheat necessary to sustain nucleate boiling at any given heat flux. Based on these findings, Corty and Foust have postulated a mechanism of bubble formation: (cavities exist on metallic surfaces and vapor is trapped in these cavities when the preceding bubble has departed or collapsed. It is this trapped vapor that acts as the nucleus for the next bubble from the same nucleation site.)

Corty and Foust measured the contact angles from bubble photographs and found that the average values fell between 40° and 60° . Then the influence of contact angle on superheat was studied for Freon 113 boiling on 4/0

polished nickel. It was found that there was shift to lower superheats with decrease in contact angles.

Bankoff [2] studied the conditions necessary for bubble nucleation in steady state boiling and developed a hydrodynamic theory for predicting the superheat required to initiate boiling. He showed that cavities required relatively low superheat and that grooves, the more common type of roughness element, were ineffective vapor traps unless very poorly wetted or steep walled.

As already mentioned, new bubbles always form from a pre-existing microscopic nucleus entrapped in a cavity in the solid surface. The formulation of Bankoff's theory of nucleation consists of an analysis of the conditions for the penetration of the liquid into a cylindrical cavity under dynamic conditions and of the variables which determine the reversal of the liquid inflow, resulting in the nucleation of a bubble.

Bankoff developed a mathematical model to predict the cavity radius corresponding to minimum superheat as

$$r_c = \left[\frac{4\mu_l k_l c_l \rho_l \sigma \cos\phi}{J^2} \left\{ \frac{T v_v (v_v - v_l)}{\lambda^2} \right\}_{\text{avg.}}^2 \right]^{1/3} .$$

Reasonable agreement with literature was shown, in view of the statistical nature of the phenomenon and the experimental uncertainties. The expression for critical cavity radius led to the following relationship.

$$(T_{w_0} - T_s) = \left[\frac{2T\lambda v_\ell (v_v - v_\ell)}{\mu_\ell k_\ell c_\ell J} \right]^{1/3} \left[\frac{\sigma \cos \phi}{v_v} \right]^{2/3}$$

which predicts the minimum superheat required to initiate boiling.

The nucleation phenomenon has been studied further by Griffith and Wallis [3]. Since bubbles originate from preexisting vapor pockets or cavities on the surface, cavity geometry is important in two ways. The mouth diameter determines the superheat necessary to initiate boiling, and its shape determines its stability once boiling has begun. Contact angle measurements by Griffith and Wallis made on clean and paraffin coated stainless steel surfaces with water showed that the contact angle varied between 20 and 110 degrees for temperatures from 20°C to 170°C.

Additional experiments performed by boiling water, methanol, and ethanol on different copper surfaces finished with 3/0 emery confirmed that a single dimension of length was sufficient to characterize a cavity, and presumably, the gross nucleation properties of the surface. For surfaces made of the same material and treated in the same way, the nucleation characteristics were shown to be represented by a single plot of the number of active nucleation sites per unit area N/A versus cavity radius r_c which has to be computed theoretically, as shown in Figure 1. The relationship for cavity radius r_c as a function of fluid properties

and surface superheat

$$r_c = \frac{2\sigma T_w (v_v - v_l)}{\lambda (T_w - T_s)} \approx \frac{2\sigma T_w v_v}{\lambda (T_w - T_s)}$$

was derived by combining Gibb's equation for static equilibrium with Clapeyron's equation relating the excess temperature in the liquid to the excess pressure in the bubble.

A test was performed in which saturated liquid was boiled from a heated surface containing artificial cavities of 0.001 inches radius. Wall superheat of 20°F was observed against 3°F predicted by

$$(T_w - T_s) = \frac{2\sigma (v_v - v_l) T_w}{\lambda r_c} = \frac{2\sigma T_w}{\lambda \rho_v r_c}$$

indicating that the model upon which this equation was based is inadequate.

Hsu [4] proposed a thermodynamic model for bubble nucleation in order to determine the conditions for bubble nucleation on a boiling surface. The size range of active cavities was predicted as a function of both wall temperature and heat flux. It was shown that the maximum and the minimum effective cavity sizes, $r_{c \max}$ and $r_{c \min}$, were functions of the liquid subcooling $T_s - T_\infty$, the system pressure P , a physical property parameter A and the thickness of the superheated liquid layer δ at the nucleation site.

$$r_{c \min} < r_c < r_{c \max} = \frac{\delta}{2C_1} \left[1 - \frac{\theta_s}{\theta_w} \pm \left\{ \left(1 - \frac{\theta_s}{\theta_w} \right)^2 - \frac{4AC_3}{\delta \theta_w} \right\}^{1/2} \right]$$

Hsu explained that although it was necessary that $r_{c \min} < r_c < r_{c \max}$ for a cavity to be active, this condition was not sufficient. In case of two cavities both with favorable geometry located close to each other, only one would be favored and would always be the active site. Hence, even if the cavity size distribution for a surface were known, Hsu's nucleation theory could not be used to predict the number of active nucleation sites.

However, one outcome of the Hsu nucleation theory was a relationship for the incipience of boiling

$$(T_{w_0} - T_s) = \frac{2AC_3}{\delta} + \left[\left\{ 2(T_s - T_\infty) + \frac{2AC_3}{\delta} \right\} \left(\frac{2AC_3}{\delta} \right) \right]^{1/2}$$

which was used to compute δ from experimental data for incipient boiling. Having obtained a numerical value, Hsu proceeded by assuming that it did not change with any other heat flux. McAdams and co-workers [5] did an experimental study of nucleate boiling of water at different subcooling and pressures with various stream velocities. Their results are shown in Figure 2 as plots of theoretical incipient boiling condition θ_{w_0} versus θ_s and P , respectively. For each curve corresponding to a given stream velocity, δ was calculated from one reference experimental point, shown in

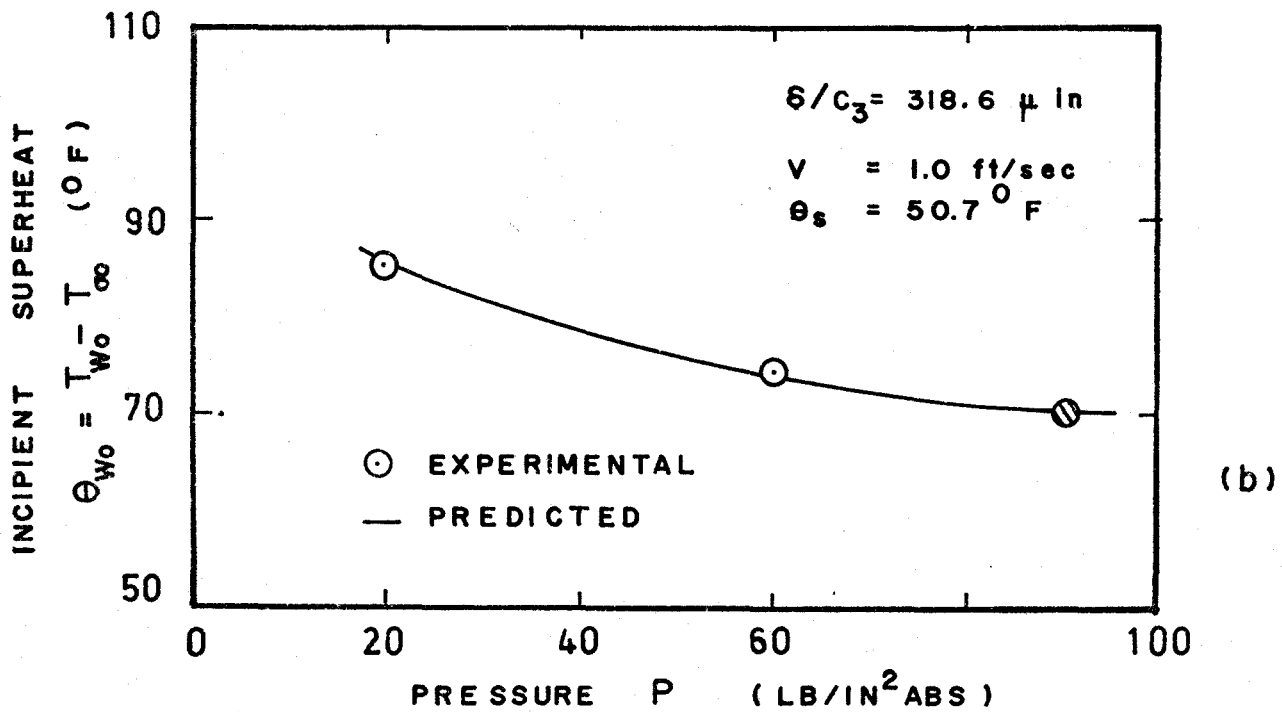
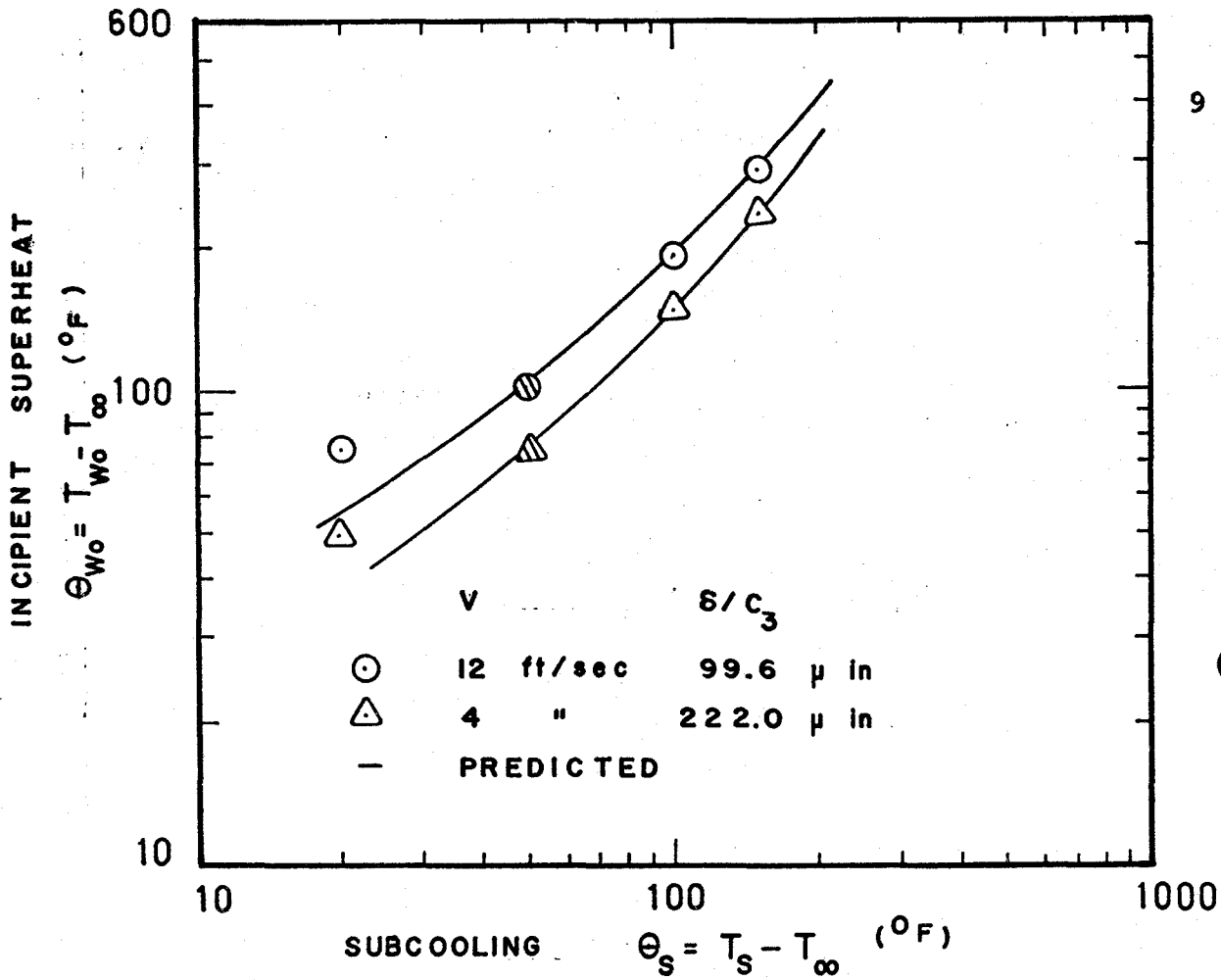


FIG. 2 (a) EFFECT OF SUBCOOLING
 (b) EFFECT OF PRESSURE ON INCIPIENT BOILING

solid circle and triangle. The comparison of theoretical and experimental values is very good.

Han and Griffith [6] studied the mechanism of heat transfer in nucleate pool boiling. They found that the temperature at which a bubble nucleated was a function of the temperature of the liquid surrounding the bubble and of the surface properties. Considering the heat transfer in the liquid adjacent to the surface as a transient conduction process, an expression for the wall superheat was developed as

$$(T_{w0} - T_s) = \frac{\theta_s + \frac{A}{r_c}}{1 - \frac{c}{2\delta}} + \theta_s$$

and the cavity radius for initiating bubble growth

$$r_c = \frac{\delta(T_{w0} - T_s)}{3\theta_{w0}} \left[1 \pm \left\{ 1 - \frac{12\theta_{w0} T_s \sigma}{(T_{w0} - T_s)^2 \delta \rho_v \lambda} \right\}^{1/2} \right]$$

Both of the preceding models for bubble nucleation require knowledge of the superheat layer thickness which has been lacking until recently. A review of two of the more recent investigations follow, since the information contained was used in the present investigation.

Judd [7] has investigated the superheated boundary layer thickness. Freon 113 was boiled on a glass plate coated with an electrically conducting oxide. The temperature

distribution in the vicinity of the plate was measured by a 0.001 inch diameter thermocouple probe. Heat flux, subcooling, and acceleration were varied so as to show the individual effects of these parameters. In accordance with previous investigations, Judd found that the thermal boundary layer thickness decreased with increasing heat flux. The superheated boundary layer thickness was found to decrease with acceleration and increase with subcooling. This investigation was accompanied by measurements of active site density and frequency of bubble emission.

Wiebe and Judd [8] undertook a further experimental study with water boiling on a horizontal copper surface for heat fluxes q/A of 20,000; 50,000 and 100,000 BTU/Hr Ft² at various levels of subcooling θ_s ranging from 0°F to 105°F. They also studied the incipient boiling heat transfer and the results were presented as the temperature difference at which incipience occurred θ_{w_0} as a function of the subcooling θ_s as shown in Figure 3. Incipient superheat θ_{w_0} calculated from Hsu's model, reproduced below, was in good agreement with θ_{w_0} from the present experiment.

Wiebe and Judd's study provided additional support to Hsu's mathematical model and presented new data for temperature distribution adjacent to a heating surface for both saturated and subcooled boiling. Increasing heat flux and decreasing subcooling results in a decreasing superheat

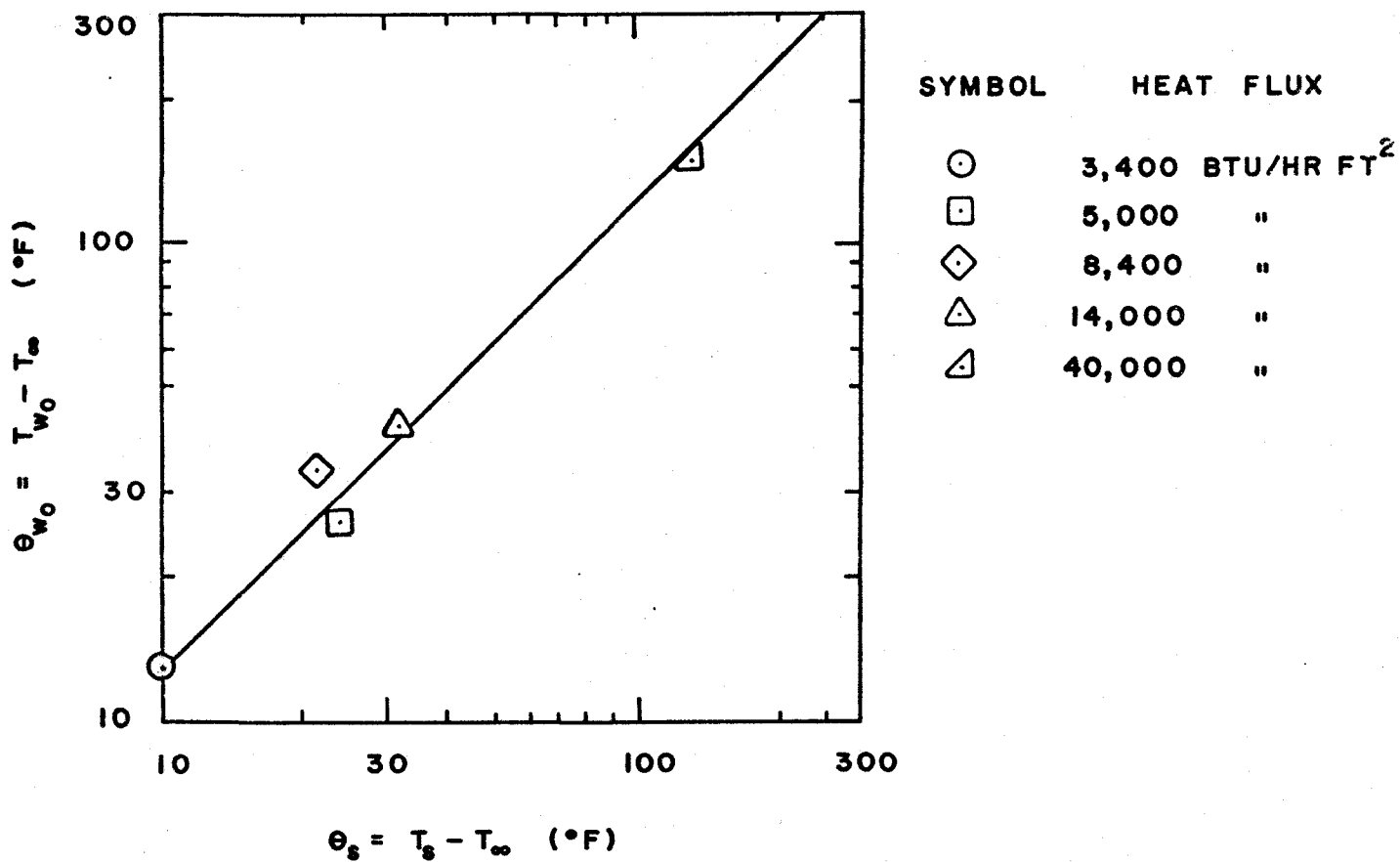


FIG.3 INCIPIENCE OF BOILING DATA

layer thickness. A relationship was shown to exist between superheat layer thickness δ and bubble flux density (N/A) f which was influenced by both heat flux q/A and subcooling $T_s - T_\infty$. This relationship was further confirmed by analysis of Judd's earlier data for Freon 113 boiling on a glass surface. The temperature profiles obtained near the heating surface enabled the superheat layer thickness to be evaluated, resulting in a correlation of heat transfer coefficient h versus superheat layer thickness δ which was independent of subcooling.

CHAPTER III

THEORETICAL CONSIDERATIONS

This section presents the derivation of four expressions for the temperature difference $\theta_{w*} = T_{w*} - T_{\infty}$ enabling the prediction of the conditions at which bubble nucleation from a cavity of radius r_c should occur, according to the models proposed by Bankoff, Griffith and Wallis, Hsu, and Han and Griffith. In essence, the authors mathematical analyses have been reproduced using a consistent set of nomenclature. It is ultimately intended to compare the expressions derived with experimental results which will be presented later in order to determine the best model for predicting bubble nucleation.

3.1 BANKOFF MODEL

Bankoff developed a theory for predicting the superheat required for initiation of boiling, based on an approximate solution of the equations for the rate of penetration of the liquid into a surface roughness element.

Bankoff considered a cylindrical cavity from which the gaseous phase could not be completely swept out by mechanical means. Boiling was assumed to have proceeded long enough for any air to have been displaced from the cavity by dilution. Once a bubble disengaged, the liquid close to it came in contact with the surface. This liquid would be saturated or subcooled, depending on the system. The disengaging bubble was essentially at the liquid pressure. Hence the residual vapor bubble began to collapse by condensing into the cavity. If the liquid were sufficiently subcooled, the bubble wall temperature would never become great enough to produce equilibrium, and the liquid would fill the cavity completely, thereafter inactivating it. If, however, the liquid were near saturation, the bubble wall temperature would approach the saturation temperature of the vapor, and the collapse velocity would decrease rapidly.

As the liquid advances into the capillary, it receives heat both from the condensation of vapor at the vapor liquid interface and by conduction of heat from the cavity walls. If the advance is quite rapid, the interface

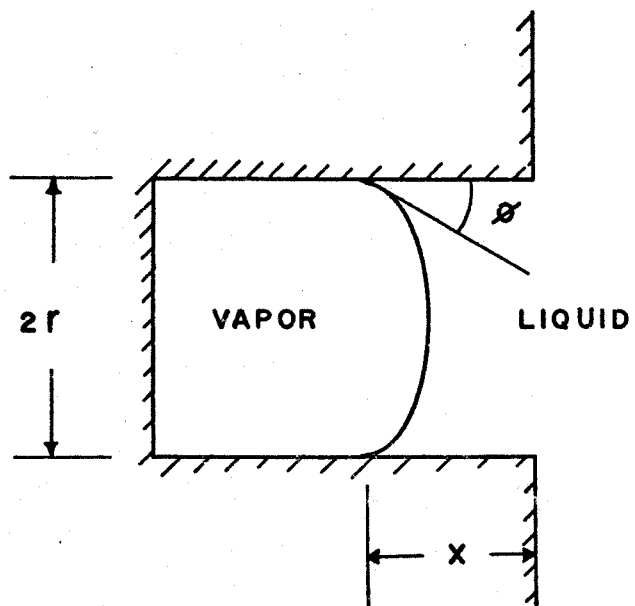


FIG. 4 MODEL FOR LIQUID PENETRATION

may become superheated, and the pressure of the vapor may approach close to the pressure required for static equilibrium. At this point the advance of the interface depends on the ability of the liquid to conduct the heat away which is limited by the velocity of the temperature wave. However, if the cavity is small enough, the velocity of the interface will be governed by the viscous drag rather than by the rate of heat conduction from the interface. The velocity of the temperature wave is about the same as the velocity of the interface. The average interface temperature approaches that of the walls well before one diameter is traversed, so that reversal of the direction of interface travel and subsequent nucleation is possible.

In the following analysis, only longitudinal temperature distribution is considered. Immediately after bubble disengagement, the interface is assumed to lie at the mouth of the cavity. The cavity is assumed to be cylindrical of radius r . Let the distance travelled by the interface in time t be x , Figure 4. At $t=0$

$$x = 0$$

$$\frac{dx}{dt} = v = 0$$

$$T_i = T_s \quad (\text{assume}) \quad .$$

Neglecting the inertial effects in the small cavity, a pressure balance requires that the pressure difference across the interface be equal to the frictional drag, given by Poiseuille's equation. Hence,

$$P_v - P_\ell = \frac{2\sigma\cos\phi}{r} - \frac{8Vx\mu}{r^2} \quad (3-1)$$

The Clausius Clapeyron equation with average values of the physical properties is

$$P_v - P_\ell = \left[\frac{\lambda}{T(v_v - v_\ell)} \right]_{\text{avg}} J(T_i - T_s) \quad (3-2)$$

A close approximate solution for the interface temperature is given by assuming that all the heat from the source is contained in one relaxation length, where $\ell \approx 2\sqrt{\alpha t}$. Assuming a uniform temperature gradient through the relaxation length, a heat balance gives

$$T_i - T_s = \frac{\lambda \rho_v x}{\sqrt{\alpha t} \rho_\ell c_\ell} \quad (3-3)$$

and the equilibrium interface superheat, the superheat at which reversal of the liquid penetration will occur, is given by

$$T_{i_0} - T_s = T_{w_0} - T_s = \frac{2\sigma\cos\phi}{Jr} \left[\frac{T(v_v - v_\ell)}{\lambda} \right]_{\text{avg}} \quad (3-4)$$

Since T_i is assumed to be equal to T_w , combining equations (3-1) and (3-2)

$$\xi = \frac{T_w - T_s}{T_{w_0} - T_s} = 1 - \frac{A}{r} \eta \frac{d\eta}{d\tau} \quad (3-5)$$

where

$$A = \frac{4\alpha\mu}{\sigma \cos\phi}$$

$$\eta = \frac{x}{r}$$

$$\tau = \frac{\alpha t}{r^2} .$$

From equation (3-3),

$$\xi = \frac{B\eta r}{\sqrt{\tau}} \quad (3-6)$$

where

$$B = \frac{J}{2\sigma\rho_l c_l \cos\phi} \left[\frac{\lambda^2}{T v_v (v_v - v_l)} \right]_{\text{avg}} .$$

Equations (3-5) and (3-6) combine to form a non-linear, first-order differential equation:

$$\frac{1}{2} \frac{A\eta}{r} \frac{d\eta}{dy} = y - B\eta r \quad (3-7)$$

where

$$y = \sqrt{\tau} .$$

Dimensionless displacement η can be expanded into a power series about the origin. If this series is substituted into the above equation and the coefficients evaluated, the solution of equation (3-7) satisfying the initial condition

$$\eta = 0 \quad \text{at} \quad y = 0$$

is

$$\eta = C \cdot y$$

where C satisfies

$$\frac{AC^2}{2r} + rBC - 1 = 0 .$$

Solving

$$r = \frac{1 \pm \sqrt{(1 - 2ABC^3)}}{2BC} . \quad (3-8)$$

Since A, B and C are always real and positive, for a real solution to exist for a particular cavity,

$$2ABC^3 \leq 1$$

and in the limit

$$c = \left(\frac{1}{2AB}\right)^{1/3}$$

whence

$$r_c = \frac{1}{2BC} = \left(\frac{A}{4B^2}\right)^{1/3}$$

and

$$r_c = \left[\frac{4\mu_\ell k_\ell c_\ell \rho_\ell \sigma \cos\phi}{J^2} \left\{ \frac{T v_v (v_v - v_\ell)}{\lambda^2} \right\}_{\text{avg.}}^2 \right]^{1/3} \quad (3-9)$$

Combining with equation (3-4), the incipient superheat is given by

$$(T_{w_0} - T_s) = \left[\frac{2T\lambda v_\ell (v_v - v_\ell)}{\mu_\ell k_\ell c_\ell J} \right]^{1/3} \left[\frac{\sigma \cos\phi}{v_v} \right]^{2/3} \quad (3-10)$$

This is the superheat at which the first cavity will become active on an infinite surface containing cylindrical cavities of all possible radii. However, for a surface containing only one cavity of known radius r_c , the temperature difference at which the cavity will become active is given by

$$\begin{aligned} \theta_{w^*} &= T_{w^*} - T_\infty \\ &= \frac{2\sigma \cos\phi}{J r_c} \left[\frac{T(v_v - v_\ell)}{\lambda} \right]_{\text{avg.}} + \theta_s \quad (3-11) \end{aligned}$$

3.2 GRIFFITH AND WALLIS MODEL

Griffith and Wallis investigated the adequacy of a simple model of bubble nucleation formulated by considering an idealized conical cavity under isothermal conditions. In a conical cavity with the bubble already in it, it may be assumed that the contact angle between the liquid and the solid is 90 degrees. When the bubble reaches the lip of the cavity, its radius of curvature begins to decrease with increasing bubble volume. When the bubble finally projects beyond the cavity with a hemispherical shape, any further increase in volume results in an increased radius of curvature. This minimum radius of curvature, called the critical radius r_c , is equal to the radius of the cavity mouth; and this radius determines the wall superheat necessary to initiate a bubble. For a wide range of cavity geometries and contact angles, this is the only dimension which needs to be specified to determine the superheat (Figure 5).

The condition for static, mechanical equilibrium of a curved vapor interface in a uniformly superheated liquid is

$$P_v - P_l = \frac{2\sigma}{r} \quad (3-12)$$

When the nucleus is at equilibrium, the pressure and the temperature of the vapor must correspond to the saturation

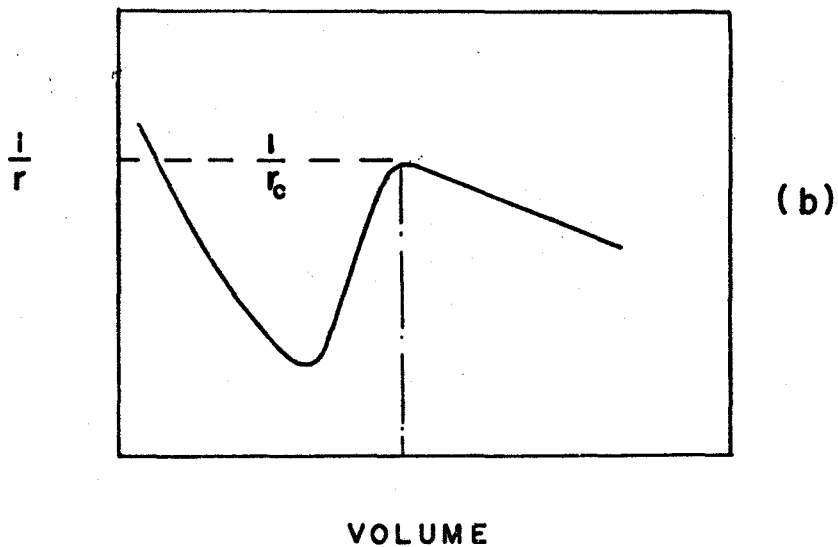
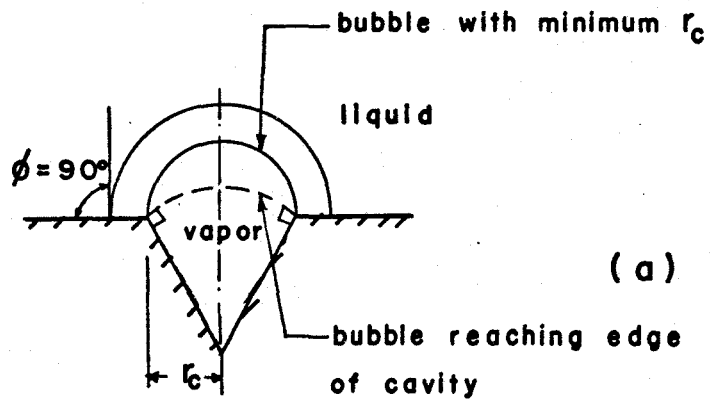


FIG. 5 NUCLEATION AT CONICAL CAVITY WITH 90° CONTACT ANGLE

conditions; that is, the vapor must be at the saturation temperature corresponding to its pressure. In order that there be no net heat flow across the vapor liquid interface, the liquid must be at the same temperature as the vapor. Therefore, the liquid is superheated. The excess temperature in the liquid can be related to the excess pressure in the bubble by the Clapeyron equation as

$$\frac{P_v - P_l}{T_w - T_s} = \frac{\lambda}{T_w (v_v - v_l)} \quad (3-13)$$

Combining equations (3-12) and (3-13),

$$(T_w - T_s) = \frac{2\sigma T_w}{\lambda \rho_v r_c} \quad (3-14)$$

and the minimum temperature difference necessary for bubble growing from a cavity of mouth radius r_c is

$$\theta_{w*} = (T_{w*} - T_\infty) = \frac{2\sigma T_w}{\lambda \rho_v r_c} + \theta_s \quad (3-15)$$

3.3 HSU MODEL

Hsu formulated a theory of bubble nucleation based upon transient conduction in the liquid at the heat transfer surface. Hsu assumed that once boiling had begun, the surface temperature remained fairly constant and there was a bubble nucleus at the mouth of a cavity, formed by residual vapor from the preceding bubble which was trapped in the cavity. At the beginning of the bubble cycle, relatively cool bulk liquid at temperature T_{∞} surrounds the nucleus at an active cavity. As time passes, the cool liquid is warmed up through the transient conduction process, and the thickness of the superheated liquid layer adjacent to the surface, called thermal layer, grows (Figure 6).

The thermal layer, however, cannot grow indefinitely, inasmuch as the ultimate thermal layer thickness is governed by eddy diffusivity and turbulence which tend to hold the temperature constant at the bulk temperature T_{∞} beyond a certain distance from the surface. Assume that such a limiting thermal layer δ exists such that for $y < \delta$ molecular transport prevails, while for $y \geq \delta$ the temperature remains at T_{∞} . For a transient conduction phenomenon, the mathematical model can be derived as follows:

$$\frac{\partial \theta}{\partial t} = \alpha \left(\frac{\partial^2 \theta}{\partial x^2} \right) \quad (3-16)$$

where

$$\theta(x,t) = T(x,t) - T_{\infty} .$$

The boundary conditions are

$$\theta(x,0) = 0 ,$$

$$\theta(0,t) = 0 ,$$

and for $t > 0$

$$\theta(\delta,t) = \theta_w .$$

The temperature profile $\theta(x,t)$ for constant θ_w is given as

$$\xi = \frac{\theta}{\theta_w} = \eta + \frac{2}{\pi} \sum_{n=1}^{\infty} \frac{\cos n\pi}{n} \sin n\pi\eta e^{-n^2\pi^2\tau} \quad (3-17)$$

where

$$\tau = \frac{\alpha t}{\delta^2}$$

$$\eta = \frac{x}{\delta} .$$

Because of the statistical nature of the turbulence, superheat layer thickness δ actually varies, and even at a given nucleation site the bubble growth rate fluctuates over a wide range.

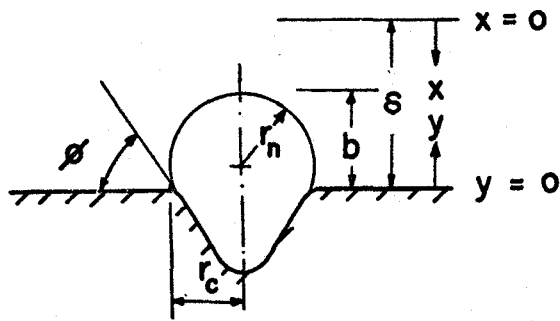


FIG. 6 BUBBLE NUCLEUS AT CAVITY MOUTH

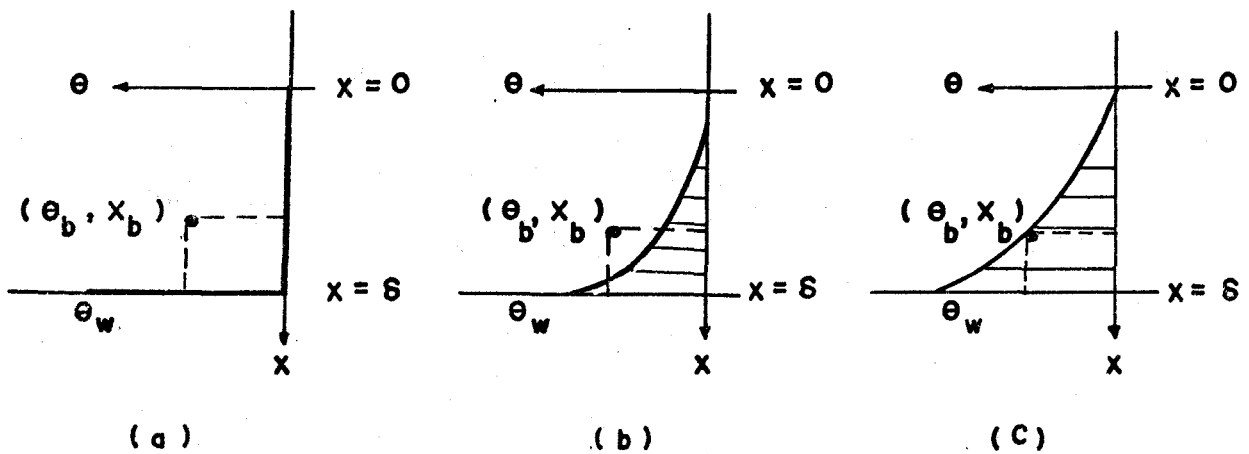


FIG. 7 MODEL FOR TEMPERATURE PROFILES

The bubble nucleus will not grow unless the surrounding liquid is warmer than the bubble temperature so that there is a net heat flux into the bubble to provide the heat of vaporization. When the bubble starts to grow, the waiting period ends.

The end of the waiting period is reached when $\theta(x,t)$ equals θ_b at $x_b = \delta - b$. The history of the waiting period is depicted by Figures 7(a), (b) and (c). Figure 7(a) shows the temperature profile at the beginning of the waiting period. Figure 7(b) represents the situation during the waiting period; the temperature profile is still below the criterion $\theta = \theta_b$ at $x_b = \delta - b$. Figure 7(c) shows the end of the waiting period when the liquid temperature distribution passes the point (θ_b, x_b) .

The surface superheat for a cavity of radius r_c is obtained, by combining the Clausius-Clapeyron equation for superheat with the Gaussian expression for surface tension, as

$$\theta_w - \theta_s = \frac{2\sigma T_s}{\lambda \rho_v r_c} \quad (3-18)$$

and so the bubble temperature is

$$\theta_b = \theta_s + \frac{2\sigma T_s}{\lambda \rho_v r_n} \quad (3-19)$$

Considering the bubble as a truncated sphere :

$$b = \left(\frac{1 + \cos\phi}{\sin\phi} \right) r_c = C_1 r_c ,$$

$$r_n = \frac{r_c}{\sin\phi} = C_2 r_c ,$$

and

$$r_n = \frac{b}{C_3} \quad \text{where} \quad C_3 = \frac{C_1}{C_2} .$$

Applying the condition for the end of the waiting period ,

$$r_n = \frac{\delta - x_b}{C_3} . \quad (3-20)$$

Combining equations (3-19) and (3-20) ,

$$\theta_b = \theta_s + \frac{2\sigma T_s}{\lambda \rho_v \left(\frac{\delta - x_b}{C_3} \right)} . \quad (3-21)$$

In dimensionless form this equation becomes :

$$\begin{aligned} \xi_b = \frac{\theta_b}{\theta_w} &= \xi_s + \frac{2\sigma T_s C_3}{\lambda \rho_v \delta \theta_w} \left(\frac{1}{1 - \eta_b} \right) \\ &= \xi_s + \frac{AC_3}{\delta \theta_w} \left(\frac{1}{1 - \eta_b} \right) \end{aligned} \quad (3-22)$$

where

$$\xi = \frac{\theta}{\theta_w}$$

$$\eta_b = \frac{x_b}{\delta}$$

$$A = \frac{2\sigma T_s}{\lambda \rho_v} .$$

Whenever equation (3-22) is satisfied, this marks the end of the waiting period.

Figure 8 shows the temperature profiles given by equation (3-17) in the dimensionless form, ξ against η with τ as a parameter. Those cavities taking an infinitely long waiting period are the inactive ones. The intersection points of the criterion curve, ξ_b against η_b , with the diagonal line of $\xi = \eta$ are designated as A and B. These two points represent the upper and lower limits for η_b . Those cavities with η_b falling within these limits have finite waiting time and thus are effective cavities; those outside this range are ineffective ones.

The value of η_b for these limiting points can be determined by substituting $\xi_b = \eta_b$ in equation (3-22)

$$\xi_b = \eta_b = \xi_s + \frac{AC_3}{\delta \theta_w} \left(\frac{1}{1-\eta_b} \right) .$$

Rearranging and simplifying,

$$\eta_b = \frac{1}{2} \left[(1+\xi_s) \pm \left\{ (1-\xi_s)^2 - \frac{4AC_3}{\delta \theta_w} \right\}^{1/2} \right] . \quad (3-23)$$

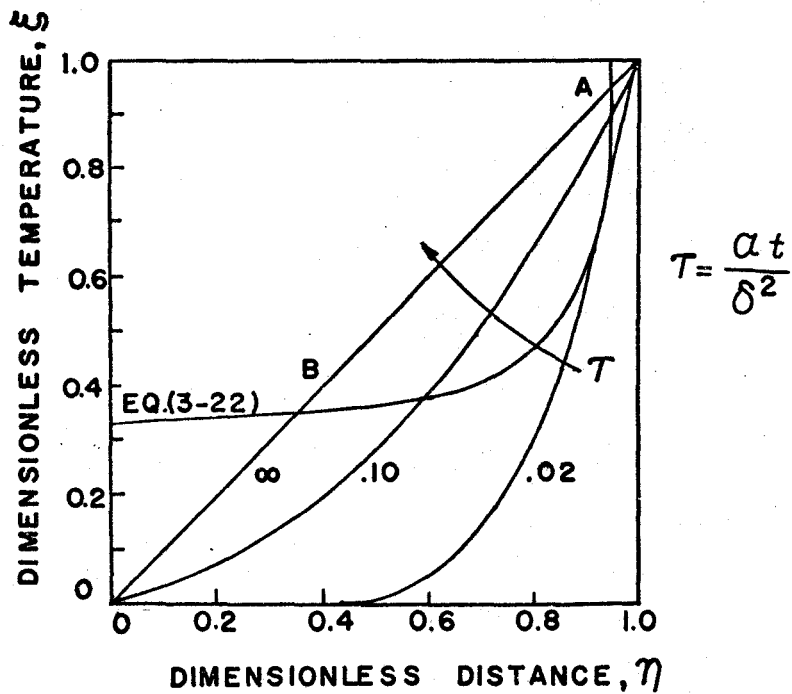


FIG. 8 TEMPERATURE PROFILE $\xi(\eta, \tau)$

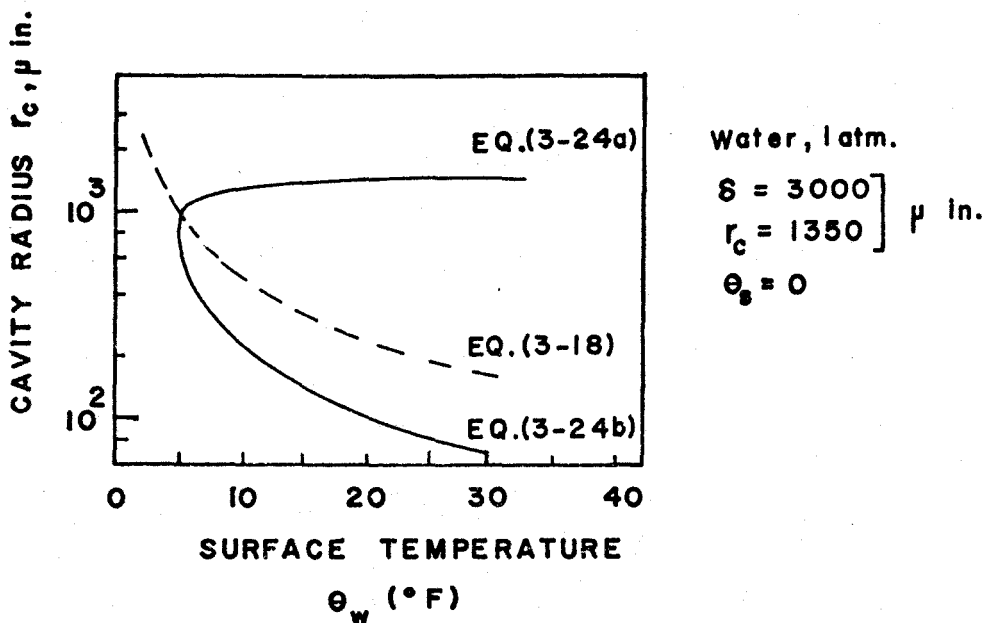


FIG. 9 ACTIVATION OF CAVITIES

Since

$$r_c = \frac{b}{C_1} = \frac{\delta(1-\eta_b)}{C_1}$$

$$r_c = \frac{\delta}{2C_1} \left[(1-\xi_s) \pm \left\{ (1-\xi_s)^2 - \frac{4AC_3}{\delta\theta_w} \right\}^{1/2} \right] \quad (3-24)$$

and,

$$r_{c_{\max}} = \frac{\delta}{2C_1} \left[1 - \frac{\theta_s}{\theta_w} + \left\{ \left(1 - \frac{\theta_s}{\theta_w} \right)^2 - \frac{4AC_3}{\delta\theta_w} \right\}^{1/2} \right] \quad (3-24a)$$

$$r_{c_{\min}} = \frac{\delta}{2C_1} \left[1 - \frac{\theta_s}{\theta_w} - \left\{ \left(1 - \frac{\theta_s}{\theta_w} \right)^2 - \frac{4AC_3}{\delta\theta_w} \right\}^{1/2} \right] \quad (3-24b)$$

It is, therefore, necessary that $r_{c_{\min}} < r_c < r_{c_{\max}}$ for a cavity to be an active one. A plot of r_c versus θ_w is given in Figure 9.

If the heating surface has no cavities other than one particular site viz. an artificial cavity, and if θ_w is replaced by the measured value θ_{w^*} , then from above

$$r_c = \frac{\delta}{2C_1} \left[1 - \frac{\theta_s}{\theta_{w^*}} + \left\{ \left(1 - \frac{\theta_s}{\theta_{w^*}} \right)^2 - \frac{4AC_3}{\delta\theta_{w^*}} \right\}^{1/2} \right] \quad (3-25)$$

On simplification

$$\theta_{w^*} = T_{w^*} - T_\infty = \frac{\theta_s + \frac{A \sin\phi}{r_c}}{1 - \left(\frac{1+\cos\phi}{\sin\phi} \right) \frac{r_c}{\delta}} \quad (3-26)$$

This is the relation which will be used in the comparison of saturated and subcooled boiling data, in which δ is obtained

from Wiebe's plot of heat flux versus extrapolated superheat layer thickness for water boiling on a copper surface.

It is evident from equation (3-24) that no cavity will be effective if

$$\left[\left(1 - \frac{\theta_s}{\theta_w} \right)^2 - \frac{4AC_3}{\delta\theta_w} \right] < 0 \quad .$$

A condition for incipient boiling can be derived from this recognizing the fact that no sustained boiling exists if

$\theta_w < \theta_{w_0}$. And hence,

$$\theta_{w_0} = \theta_s + \frac{2AC_3}{\delta} + \left[\left(2\theta_s + \frac{2AC_3}{\delta} \right) \left(\frac{2AC_3}{\delta} \right) \right]^{1/2} \quad . \quad (3-27)$$

This equation shows that if superheat layer thickness δ is known, the incipience of boiling can be predicted for a given pressure and subcooling or, vice versa. This, in fact, is the relationship which Wiebe and Judd used in comparing their incipient boiling data as discussed above.

3.4 HAN AND GRIFFITH MODEL

Han and Griffith formulated a theory for bubble nucleation using much the same analysis as Hsu used. A bubble was assumed to originate from a small gas filled cavity on the heating surface whenever the surrounding fluid was heated to a sufficiently high temperature. Han and Griffith considered the temperature distribution in the vicinity of the surface once a bubble has departed and cold liquid replaced it. The initial and boundary conditions are

$$\left. \begin{array}{ll} T = T_w & \text{at } x = 0 \\ T = T_\infty & \text{at } x > 0 \end{array} \right\} t = 0$$

$$\left. \begin{array}{ll} T = T_w & \text{at } x = 0 \\ T = T_\infty & \text{at } x = \infty \end{array} \right\} t > 0 .$$

Assuming transient heat conduction, the solution is

$$T - T_\infty = (T_w - T_\infty) \operatorname{erfc} \frac{x}{2\sqrt{\alpha t}} \quad (3-28)$$

and

$$\left(\frac{\partial T}{\partial x}\right)_{x=0} = - \frac{T_w - T_\infty}{(\pi \alpha t)^{1/2}} .$$

The temperature distribution at any instant is found to vary approximately linearly from the wall to $x = \delta$. Beyond this the fluid is unaffected by the temperature of the wall. The thickness of the thermal layer is defined from the above relation as

$$\delta = (\pi \alpha t)^{1/2} .$$

Before the growth, the bubble at the mouth of a cavity of radius r_c is in a hydrostatic equilibrium defined by

$$P_v - P_s = \frac{2\sigma}{r_c} .$$

Applying Clausius-Clapeyron relation for thermodynamic equilibrium

$$P_v - P_s = \frac{T_v - T_s}{T_s} \cdot \frac{\lambda}{\frac{1}{\rho_v} - \frac{1}{\rho_l}} \approx \frac{(T_v - T_s) \rho_v \lambda}{T_s} .$$

Eliminating $P_v - P_s$ from the above equations

$$T_v - T_s = \frac{2\sigma T_s}{\rho_v \lambda r_c} .$$

During the initial period of growth, the bubble can be treated as an insulated hemisphere of radius r_c . From potential flow theory and fluid flow analogy, the potential

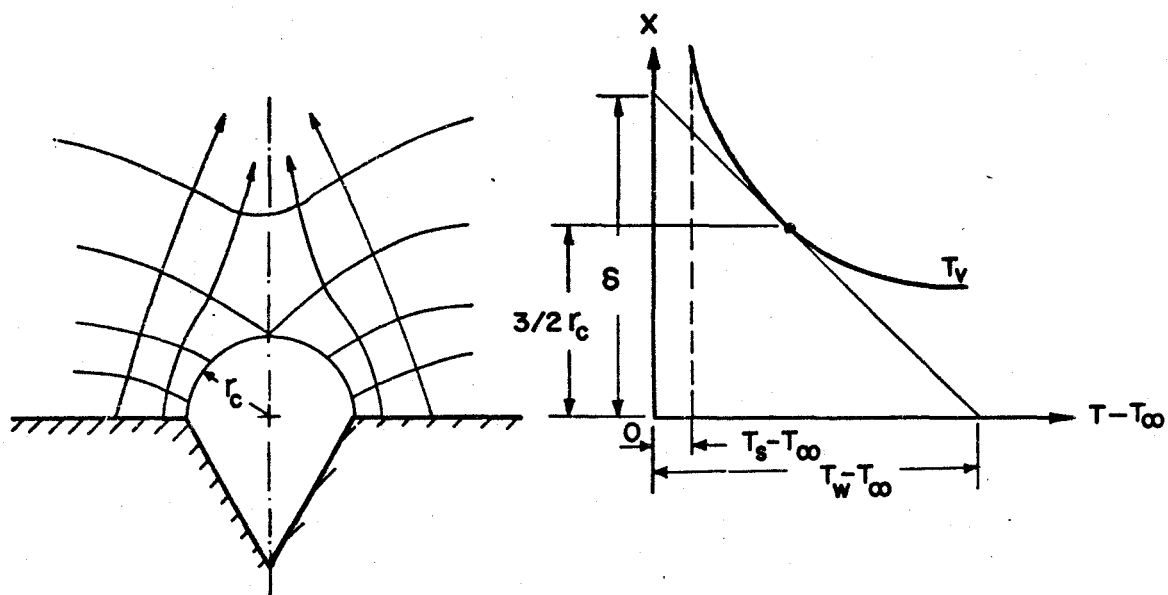


FIG. 10 TEMPERATURES OF FLUID AND BUBBLE NEAR A HEATING SURFACE .

line in fluid flow is just equivalent to the isothermal line in heat conduction. The distance of an isothermal line passing through the top point of a waiting bubble is $3/2 r_c$ from the heating surface when measured on the flat portion of the isothermal surface (Figure 10). Liquid temperature at $x = 3/2 r_c$ is

$$\begin{aligned} T_\ell &= (T_w - T_\infty) \left[1 - \frac{3/2 r_c}{\delta} \right] + T_\infty \\ &= T_w - (T_w - T_\infty) \frac{3r_c}{2\delta} . \end{aligned}$$

Equating T_v with T_ℓ

$$T_s + \frac{A}{r_c} = T_w - (T_w - T_\infty) \frac{3r_c}{2\delta}$$

where $A = 2\sigma T_s / \lambda \rho_v$. On simplification

$$\theta_w = T_w - T_\infty = \left[(T_s - T_\infty) + \frac{A}{r_c} \right] / \left[1 - \frac{3r_c}{2\delta} \right] \quad (3-29)$$

and replacing θ_w with θ_{w*}

$$\theta_{w*} = T_{w*} - T_\infty = \left(\theta_s + \frac{A}{r_c} \right) / \left(1 - \frac{3r_c}{2\delta} \right) . \quad (3-30)$$

As in Hsu's model, this is the basic relation which will be used in the comparison of saturated and subcooled boiling data.

C H A P T E R I V

EXPERIMENTAL APPARATUS

The test apparatus is described for convenience under different headings as follows:

4.1 DESIGN CRITERIA

The apparatus constructed was capable of:

1. Boiling liquids up to a maximum heat flux of 30,000 BTU/Hr Ft².
2. Subcooling the bulk liquid by about 30°F at the maximum heat flux condition.
3. Measuring temperatures in the close vicinity of an artificial nucleation site.
4. Allowing visual observation of the artificial nucleation site in order to determine the conditions under which a bubble was nucleated.

4.2 TEST ASSEMBLY

As stipulated, the aim of the study was to investigate the nucleation phenomenon from an artificial site in pool boiling. The test assembly constructed to achieve this purpose was comprised of a transparent sleeve surrounding a horizontal heating surface which enabled viewing from outside. A sectional view of the complete test assembly is shown in Figure 11. The hollow plexiglass sleeve 4 inches internal diameter by 1/4 inch thick by 6 inches high and the heating surface, a copper disc 4 inches diameter and 3/8 inch thick may be seen. A hole drilled through the center of the copper disc contained a stainless steel capillary tube 2 inches long by 0.018 inch outside diameter and 0.0084 inch inside diameter, soldered in position with its upper end flush with the surface of the disc. This "orifice" at the center of the heating surface represented an artificial nucleation site in the study. The capillary tube was protected by another stainless steel tube 3/16 inch outer diameter by 2-1/2 inches long, silver soldered on to the copper disc. The plexiglass sleeve was press fitted on to the copper disc by means of a 'O' ring seal set in a groove in the edge of the disc.

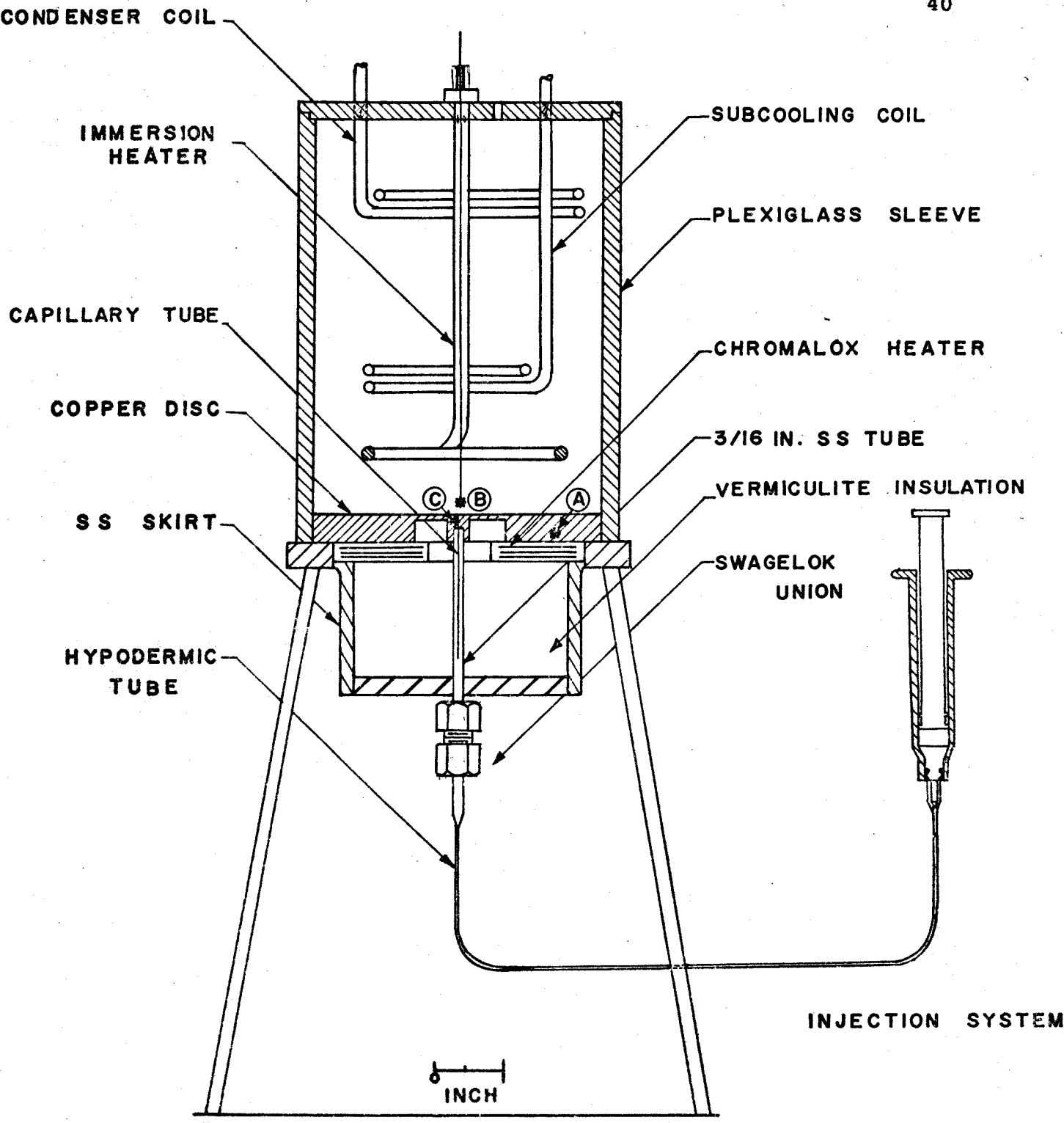


FIG. II SECTIONAL VIEW OF TEST ASSEMBLY

4.3 HEATING SYSTEM

The heating system consisted of a Chromalox ring heater (350 watts, 240 volts, 15 amperes) secured at the bottom surface of the copper disc by Thermon standard grade heat transfer cement for improved heat flow. A stainless steel skirt 3-3/8 inches outside diameter by 1-3/4 inches long and 3/16 inch thick, was fitted around the heater and closed at the other end by a disc of low conductivity material. The space inside the skirt was packed with insulating material, viz. vermiculite, to prevent any appreciable heat loss from the heater to the ambient. The bulk heater was an immersion heater 3/16 inch in diameter with a total of 6 square inches of heating surface. The electrical connections are shown schematically in Figure 12.

4.4 INJECTION SYSTEM

The injection system was comprised of a hypodermic syringe connected to the 3/16 inch stainless steel tube by a stainless steel capillary tube 1/16 inch outer diameter. The syringe contained water which could be injected through the orifice into the system in order to make sure that no air was locked up into the system.

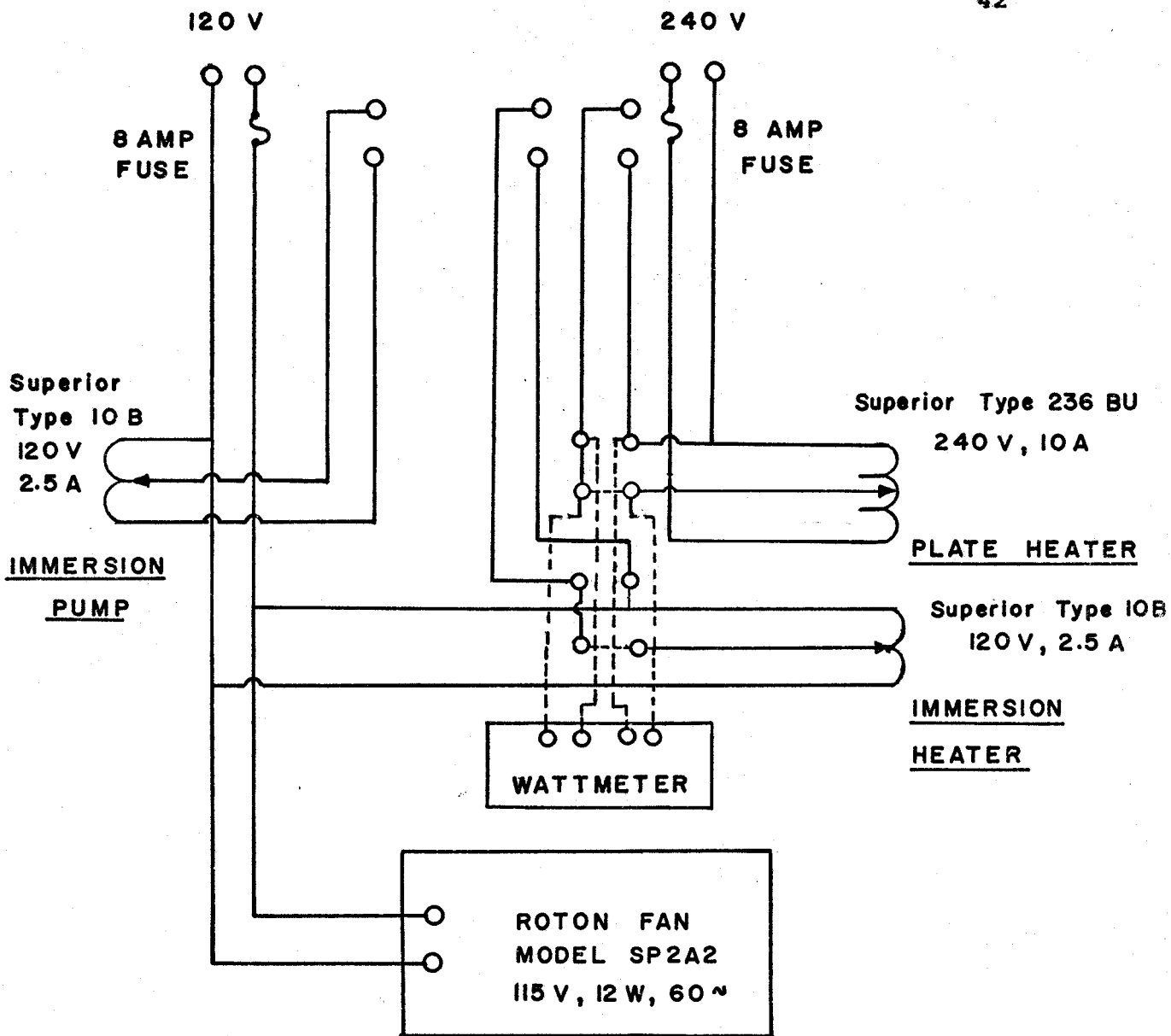


FIG. 12 ELECTRICAL CONNECTIONS

4.5 COOLING SYSTEM

A condenser was constructed of 3 turns of 1/4 inch copper tube with 20 square inches of cooling surface and suspended from the cover plate. Cold water was passed through it to condense the water vapor back to the liquid phase. A copper coil with 2 turns in series with a total of 15 square inches of cooling surface was used to subcool the bulk liquid.

To restrict the amount of energy conducted from the heating surface to the artificial nucleation site, a recess was made in the underside of the heating surface, and another cooling coil of 1/8 inch copper tubing was fitted to regulate the temperature at the artificial nucleation site, as shown in Figure 13. A water bath was maintained at a desired temperature by a thermostat heater. A small immersion pump was employed to circulate the water through the cooling circuit and back to the bath.

4.5 POWER AND CONTROLS

A 240 volt 10 ampere variac delivered power to the plate heater. A wattmeter connected in the circuit (Conway Electronics, #5523802) measured the power dissipated in the heater. Two Superior type 10B variacs 120 volt 2.5 ampere supplied energy to the immersion heater in the bulk liquid and the immersion pump in the cooling section respectively.

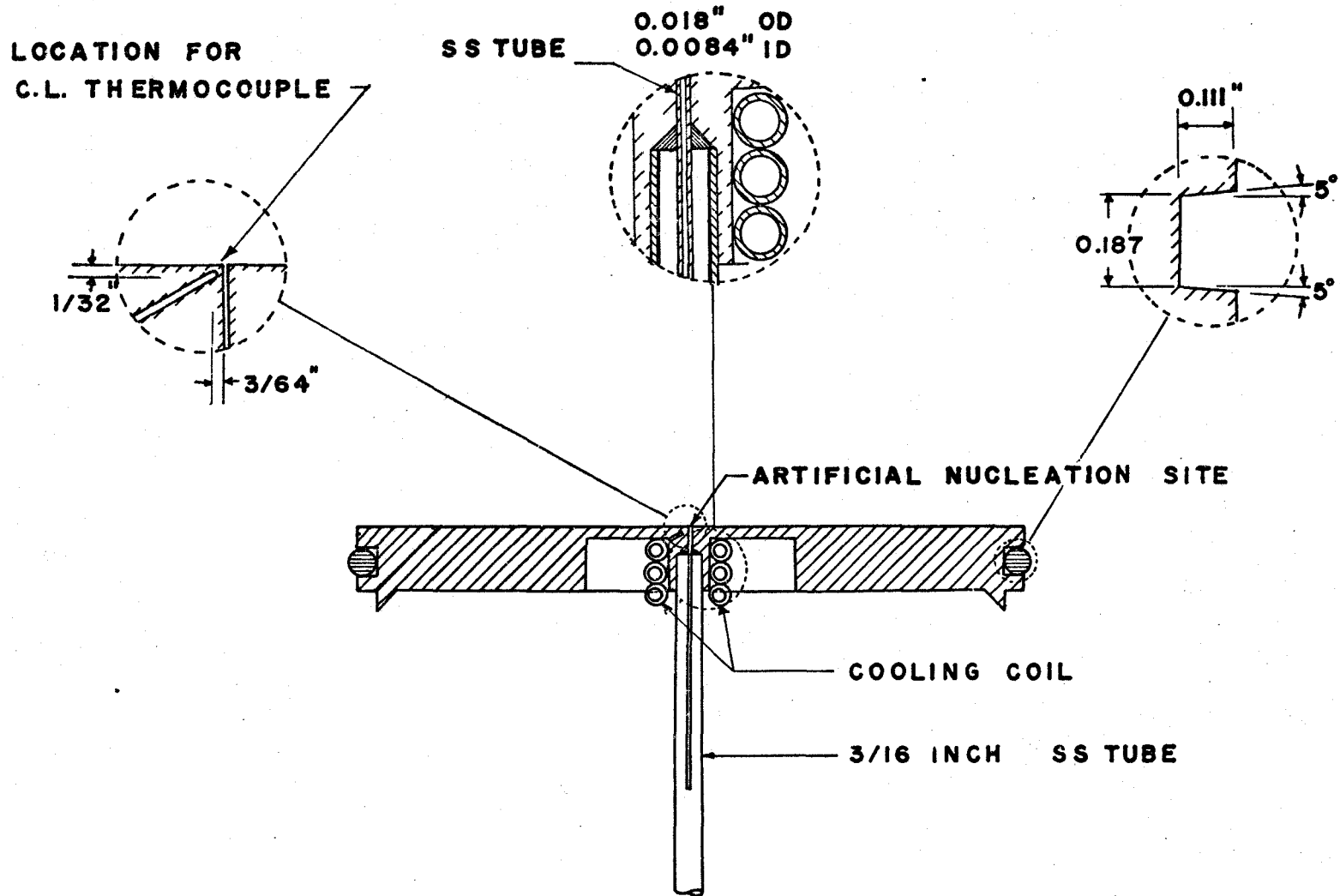


FIG. 13 COPPER HEATING SURFACE

The pump speed and hence the cooling rate was controlled by varying the current through the pump circuit. A control valve (Whitey Cat.#1RS4 Regulating Stem) was used to regulate the mains water flow rate in the subcooling circuit.

4.7 THERMOCOUPLES

Chromel-Constantan thermocouples were located at suitable places to measure the temperature as indicated in Figure 11. The thermocouples were constructed from 36 gauge fibreglass insulated wires spot welded together. A 1/16 inch hole, 1 inch long was drilled into the copper disc from the periphery towards the center ending 1/4 inch below the surface, and thermocouple 'A' was inserted into it to measure the heating surface temperature T_w . The bulk liquid temperature T_∞ was measured by thermocouple 'B' which was encased in a stainless steel capillary tube and suspended through a 3/32 inch stainless steel collar into the bulk liquid very close to the artificial nucleation site. A fine hole drilled through the underside of the copper disc, as shown in Figure 13, to reach as close to the artificial nucleation site as possible contained thermocouple 'C' which was held in place by epoxy glue. The temperature measured was referred to as the center line temperature T_{w*} , an important parameter in the present investigation. The

thermocouple was made of bare 36 gauge thermocouple wire threaded through a 1/16 inch diameter two-hole ceramic insulator. Chromel-Constantan combination was selected because EMF characteristic for the pair is approximately 36 μ volt/deg F, the maximum attainable in the temperature range under consideration.

All the thermocouples were standardized by placing them in a constant temperature environment and comparing their readings with those of a mercury-in-glass thermometer. In all cases the deviation in temperature reading was less than 1°F.

4.8 TEMPERATURE MEASURING SYSTEM

The typical thermocouple circuit is shown in Figure 14. To conserve chromel constantan lead wire, a transition was made to single strand nylon insulated thermocouple grade copper wire at an ice bath in all the thermocouple circuits. The leads were then connected to a switch board on which double pole, double throw copper knife switches directed the desired output signal to a Honeywell potentiometer (Model #2745, Serial #109178) capable of reading with an accuracy of 0.005 millivolt. In addition, the signals from the thermocouples could be fed directly to a Philips 12-Channel recorder (Model PR 4069 M/04). Recordings were taken only

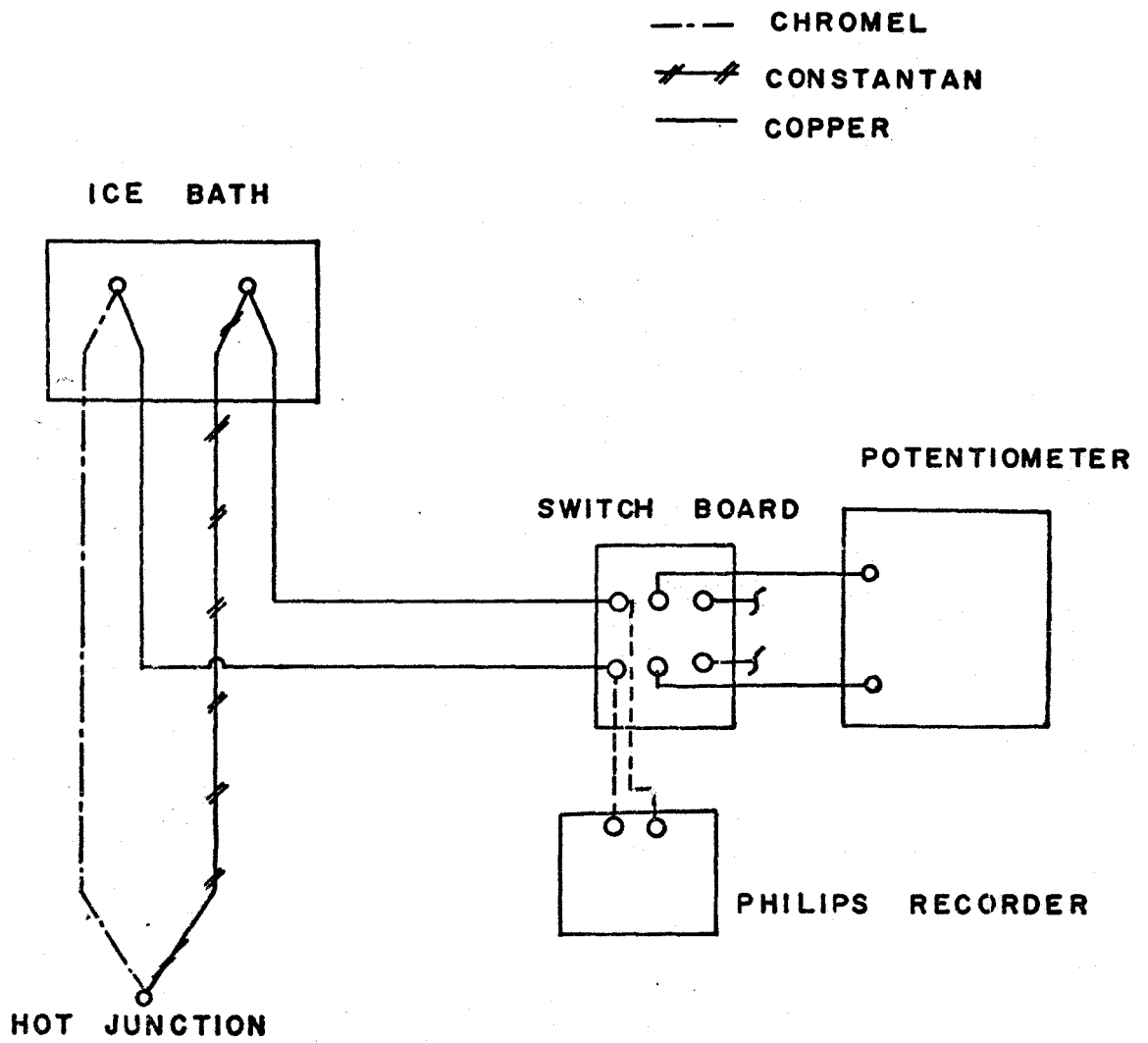


FIG. 14 THERMOCOUPLE CIRCUIT DIAGRAM

to make sure that equilibrium condition had been attained.

The final readings were taken from the precision potentiometer.

C H A P T E R V

TEST CONDITIONS

The investigation was carried out at normal atmospheric pressure, and at various subcooling and heat fluxes as summarized below.

1) Natural Convection Boiling - heat flux was increased from 3,900 BTU/Hr Ft² at suitable steps up to about 10,000 BTU/Hr Ft² beyond which nucleate boiling ensued.

2) Nucleate Boiling - in which the condition of initiation of bubble at the artificial site was sought for various heat fluxes from 11,700 BTU/Hr Ft² to 19,500 BTU/Hr Ft², and subcooling up to about 30°F.

The range of subcooling achieved for different heat fluxes in the nucleate boiling regime may be shown in a tabular form.

TABLE I

HEAT FLUX (BTU/Hr Ft ²)	SUBCOOLING		NO. OF TESTS
	MINIMUM (°F)	MAXIMUM (°F)	
11,700	0.6	27.1	25
13,700	0.4	2.6	13
15,600	0.2	32.2	21
17,600	0.2	20.1	17
19,500	21.4	32.6	6

C H A P T E R V I

TEST PROCEDURE

The apparatus was filled with about 3 inches of deionized distilled water and then the surface heater and the bulk heater were turned on. A heater power setting of about 450 watts ($19,500 \text{ BTU/Hr Ft}^2$) was established initially to heat up the apparatus quickly and this setting was left for one hour. Meanwhile the syringe was filled with degassed distilled water and the plunger was depressed several times to make certain that the system was free of any air, which was indicated by the cessation of air bubbles through the orifice. The condenser cooling water was turned on at this time.

To assure that the nucleation sites were properly activated at the beginning of each test, saturated boiling at $19,500 \text{ BTU/Hr Ft}^2$ was allowed to continue for about thirty minutes after which the power was reduced to the desired level for each subsequent test. Once the heat flux or sub-cooling was changed to a new value, it took about an hour for the system to regain the thermal equilibrium.

Following the start up procedure, water in the tank was heated to nearly 140°F . The required cooling at the artificial nucleation site was established by adjusting the cooling water flow rate by setting the speed of the immersion

pump. It was found that there were no bubbles initiated at the artificial nucleation site until the heat flux was in excess of 10,000 BTU/Hr Ft². Consequently, the heat flux settings investigated for saturated boiling were 11,700; 13,700; 15,600; 17,600 and 19,500 BTU/Hr Ft². At each heat flux level, the cooling water flow rate was so adjusted that nucleation ceased and a vapor bubble was observed to stand at the artificial nucleation site. A slight increase in the cooling rate at this stage was sufficient to eliminate the bubble at the artificial nucleation site.

Once conditions had attained steady state, as indicated by the response of the temperature recorder, the individual temperatures for the heating surface, the bulk liquid and the center line, were measured by the Honeywell potentiometer. The barometric pressure was recorded before and after each set of tests performed in one day.

A similar procedure was followed for subcooled boiling. The rate of subcooling could be controlled by the control valve installed in series with the subcooling coil.

At any heat flux, the condition for bubble initiation at the artificial nucleation site was established by a combination of both the artificial site cooling and bulk subcooling.

Once the steady state condition had been indicated by the Philips temperature recorder, the individual measurements were taken for the center line, the bulk liquid and

the heating surface temperatures. The barometric pressure was noted as before.

CHAPTER VII

RESULTS

The experimental data is presented here without much discussion since an assessment follows in Chapter VIII. The results and related uncertainty analysis appear in tabulated form in Appendices A and C.

Figure 15 is the characteristic curve for water boiling on copper surface. The natural convection and the nucleate boiling regimes are identified. The natural convection is seen to follow the correlation $Nu = 0.67 (Gr Pr)^{1/3}$. One of the well known correlations advanced by Fishenden and Saunders [9] $Nu = 0.16 (Gr Pr)^{1/3}$ is shown on the graph for comparison. Plotted on this graph are the results of Lippert and Dougall [10], and Bobst and Colver [11]. The nature of the characteristic curve obtained from the present investigation has some agreement with those by the authors mentioned above, although the reason for the discrepancy in the natural convection regime is not known.

In Figure 16 wall superheat is plotted as a function of bulk liquid subcooling at constant heat flux condition. It is found that the superheat increases first and on extrapolation approaches asymptotically to the natural convection condition (shown for the lowest heat flux)

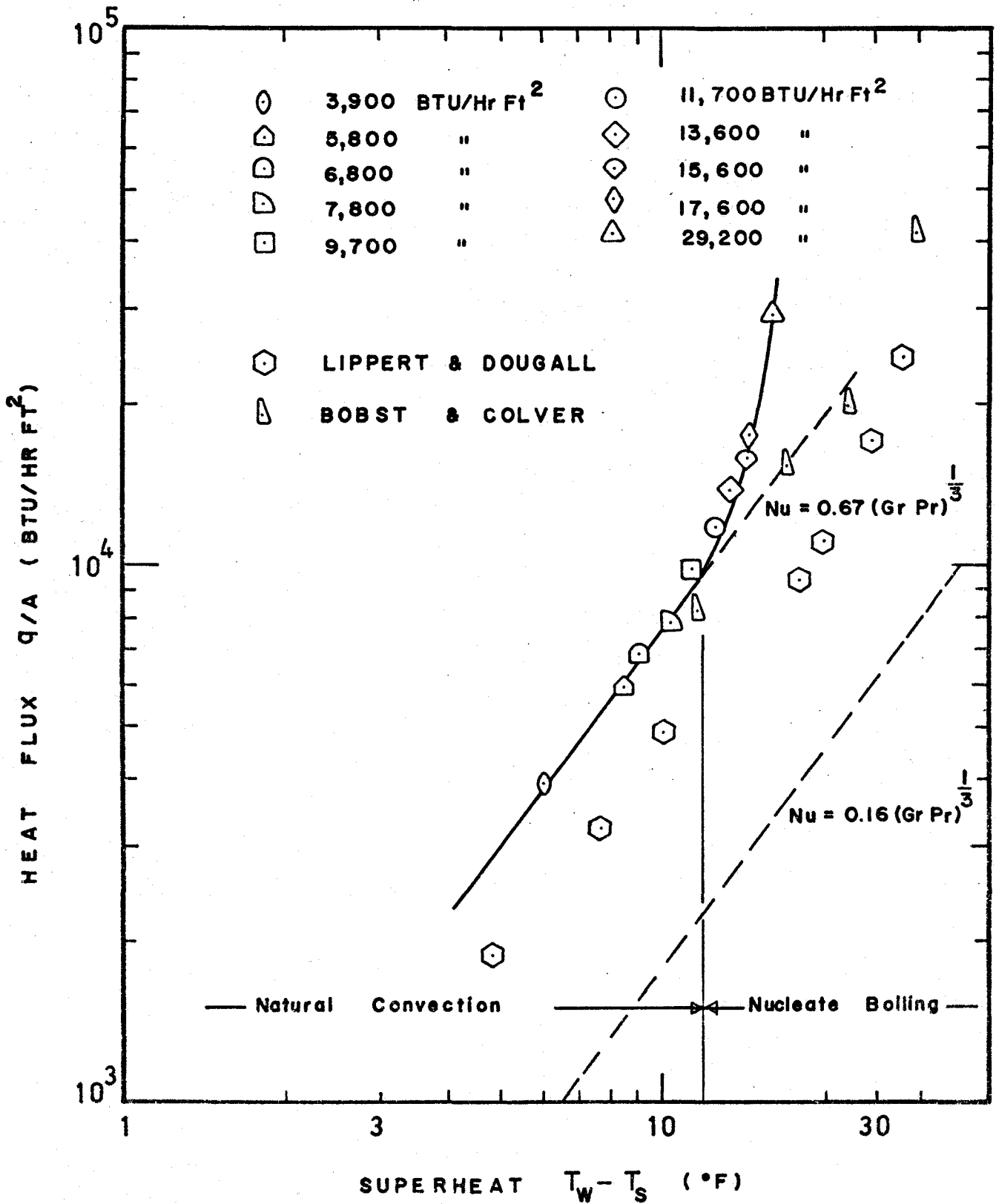


FIG. 15 HEAT FLUX — SUPERHEAT CHARACTERISTICS

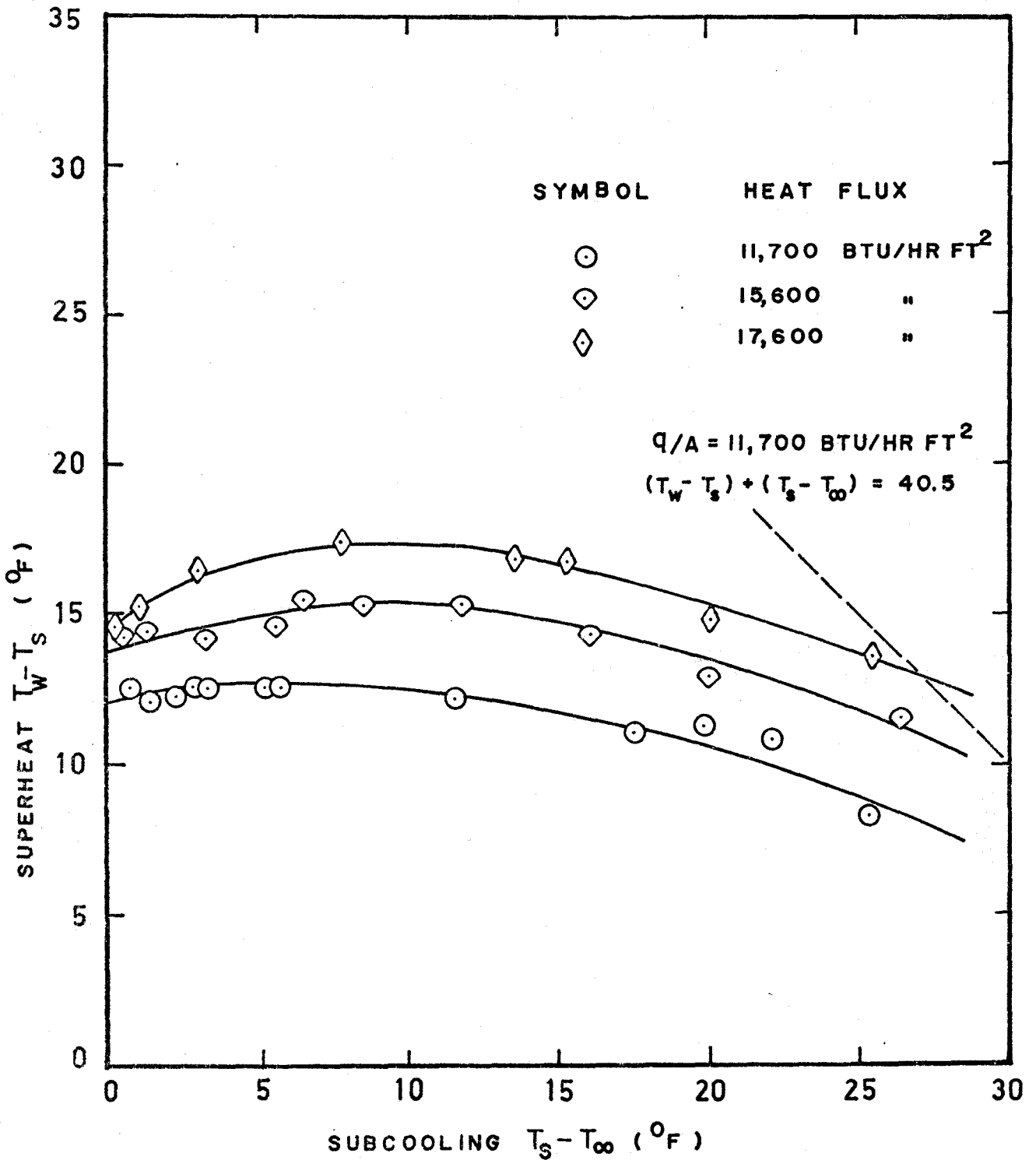


FIG. 16 VARIATION OF WALL SUPERHEAT WITH BULK SUBCOOLING.

$$\text{Nu} = 0.67 (\text{Gr Pr})^{1/3} . \quad (7-1)$$

This relation, in fact, reduces to a family of straight lines under constant heat flux condition,

$$(T_w - T_s) + (T_s - T_\infty) = \text{constant} . \quad (7-2)$$

The superheat changes with subcooling only slightly and that is why it is often claimed that nucleate boiling is insensitive to variations in the level of subcooling. Judd [12] noticed this effect and commented upon it, explaining that the slight rise in surface superheat was due to the fact that nucleate boiling became progressively less effective to transfer the heat as subcooling increased. When the subcooling is increased sufficiently, the natural convection dominates and the surface superheat decreases as subcooling increases.

The experimental data is given in tabular form as shown below.

TABLE II

q/A (BTU/Hr Ft ²)	$\theta_s = T_s - T_\infty$ (°F)	$\theta_w = T_w - T_\infty$ (°F)	$\theta_{w*} = T_{w*} - T_\infty$ (°F)
11,700	0.6	13.6	3.7 ^{$T_{w*} - T_s$} 3.1
	0.7	14.2	4.4
	0.8	12.0	5.2
	0.9	13.3	4.6
	1.0	13.7	3.4 ^{2.4}
	1.2	13.9	4.0
	1.2	11.9	3.8
	1.3	13.5	4.3
	1.4	14.0	3.3 ^{1.9}
	2.3	14.5	6.1
	2.5	14.8	6.5
	2.9	15.4	7.3
	3.2	15.8	6.7

TABLE II - continued

q/A (BTU/Hr Ft ²)	$\theta_s = T_s - T_\infty$ (°F)	$\theta_w = T_w - T_\infty$ (°F)	$\theta_{w*} = T_{w*} - T_\infty$ (°F)
11,700	3.5	16.5	9.3
	5.3	17.8	11.9
	5.8	18.5	9.8
	5.9	17.8	9.6
	11.6	23.8	18.5
	17.5	28.4	26.3
	19.9	31.1	28.6
	20.9	31.3	30.5
	21.9	31.6	30.2
	21.9	33.8	31.2
	25.2	31.3	32.1
	27.1	39.3	32.5

TABLE II - continued

q/A (BTU/Hr Ft ²)	$\theta_s = T_s - T_\infty$ (°F)	$\theta_w = T_w - T_\infty$ (°F)	$\theta_{w*} = T_{w*} - T_\infty$ (°F)
13,700	0.4	12.8	2.6
	0.4	12.9	3.2
	0.4	15.6	4.6
	0.8	14.0	3.6
	0.8	14.1	4.5
	0.9	10.7	3.3
	1.0	14.3	2.9
	1.0	14.4	4.8
	1.2	11.9	3.6
	1.2	14.8	3.4
	1.3	14.6	6.7
	1.4	14.9	5.1
	2.6	13.4	10.0

1.9

TABLE II - continued

q/A (BTU/Hr Ft ²)	$\theta_s = T_s - T_\infty$ (°F)	$\theta_w = T_w - T_\infty$ (°F)	$\theta_{w*} = T_{w*} - T_\infty$ (°F)
15,600	0.4	13.5	4.2
	0.4	15.9	3.3
	0.8	15.0	4.2
	0.9	15.1	3.0
	1.2	15.1	7.4
	1.2	15.2	3.4
	1.3	13.7	3.7
	1.3	15.4	6.2
	1.4	15.7	3.8
	2.6	13.7	10.0
	3.2	17.2	10.3
	5.6	20.1	12.7
	6.5	22.0	13.8
8.6	23.9	17.4	

TABLE II - continued

q/A (BTU/Hr Ft ²)	$\theta_s = T_s - T_\infty$ (°F)	$\theta_w = T_w - T_\infty$ (°F)	$\theta_{w*} = T_{w*} - T_\infty$ (°F)
15,600	11.8	27.0	21.5
	15.9	30.1	26.1
	19.9	32.7	30.6
	26.3	37.8	35.6
	28.0	40.0	37.7
	28.2	40.6	37.0
	32.2	42.1	40.0

TABLE II - continued

q/A (BTU/Hr Ft ²)	$\theta_s = T_s - T_\infty$ (°F)	$\theta_w = T_w - T_\infty$ (°F)	$\theta_{w*} = T_{w*} - T_\infty$ (°F)
17,600	0.2	14.6	3.2
	0.2	14.7	2.6
	0.8	15.2	2.4
	0.9	15.2	3.1
	1.0	16.1	2.4
	1.0	16.5	4.0
	1.2	14.0	3.6
	1.2	14.2	3.6
	1.2	15.5	4.4
	1.2	15.6	3.9
	1.2	15.9	3.4
	1.3	16.4	6.5
	3.0	19.5	11.1
7.8	25.3	17.7	

TABLE II - continued

q/A (BTU/Hr Ft ²)	$\theta_s = T_s - T_\infty$ (°F)	$\theta_w = T_w - T_\infty$ (°F)	$\theta_{w*} = T_{w*} - T_\infty$ (°F)
17,600	13.6	30.3	23.6
	15.2	32.0	25.5
	20.1	34.8	30.6
19,500	21.4	37.1	32.2
	25.3	40.0	37.9
	27.0	41.8	38.2
	27.4	41.3	38.8
	28.1	41.3	39.4
	32.6	46.1	44.0

CHAPTER VIII

DISCUSSION

Wiebe and Judd's correlation for heat transfer coefficient versus extrapolated superheat layer thickness is reproduced in Figure 17 for reference. The extrapolated superheat layer thickness is defined as the height of the intersection between the tangent to the temperature profile at the surface and the constant bulk liquid temperature line. Since the tangent is an "extrapolation" of the linear portion of the temperature distribution, the parameter δ is called the "extrapolated" superheat layer thickness. The heat transfer coefficient h is defined as the ratio of the heat flux to the difference between wall temperature and bulk temperature.

Bankoff's model predicts an exceptionally high value for the incipience superheat. At saturated boiling condition the value calculated by equation (3-10) is 26.6°F , which is much too high compared to the values observed in the present investigation. For the nucleation of a bubble from an artificial nucleation site 8.4×10^{-3} inches diameter, equation (3-9) predicts that the superheat should be of the order of $300,000^{\circ}\text{F}$, which is totally unreasonable. It is concluded that this model does not describe the mechanism of nucleation.

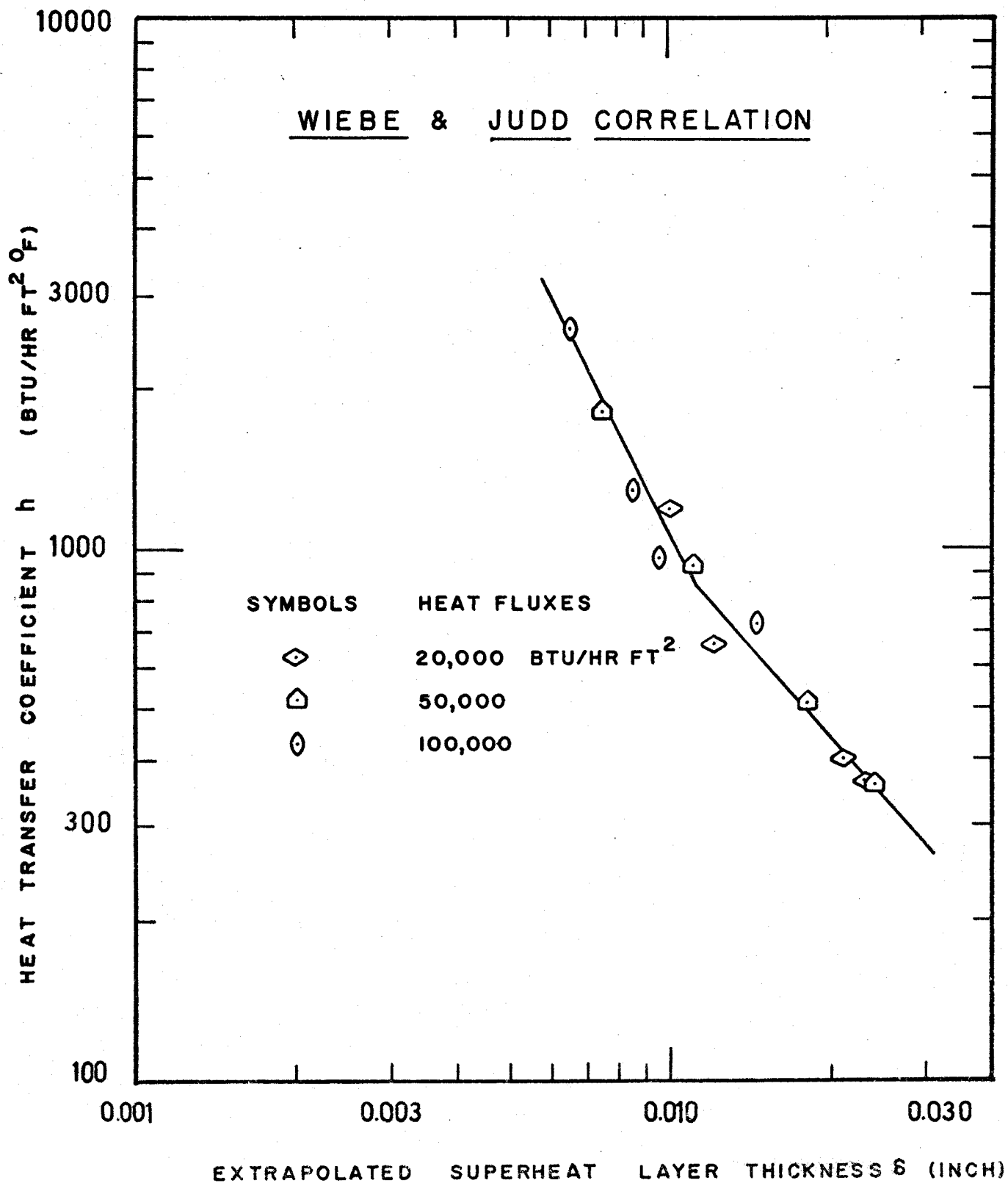


FIG. 17 SUPERHEAT LAYER THICKNESS CORRELATION

The model which Griffith and Wallis investigated is definitely an improvement on the previous model since it predicts considerably lower values for θ_{w*} . Figure 18 is a plot of θ_{w*} experimental against θ_{w*} predicted from equation (3-15). As indicated in Figure 18, the higher the system subcooling, the better the agreement with the experiment. The results are not completely satisfactory but certainly closer to the actual values. Griffith and Wallis' model underpredicts the superheat because of the unrealistic assumption that the liquid is uniformly superheated. In nucleate boiling, there is a severe temperature gradient adjacent to the heated surface and the liquid influencing the bubble nucleation is far from being uniformly superheated.

Figure 19 shows a plot of θ_{w*} experimental against θ_{w*} predicted from Hsu's model, equation (3-26), using contact angle $\phi = 53.2^\circ$. Superheat layer thickness δ is measured from Figure 17 for the corresponding heat flux. It is quite apparent that this model overpredicts the superheat. The agreement is found to be better when $\phi = 70^\circ$ is used in equation (3-26), and the results so obtained are plotted as θ_{w*} experimental versus θ_{w*} predicted in Figure 20. Rao [13] reported that for high energy surfaces, for example, copper, values or contact angle of 66° to 72° were observed. This provides additional support to our choice of the contact angle as 70° . Figure 20 shows good agreement, most of the points falling within $\pm 20\%$ of the theoretical line. This

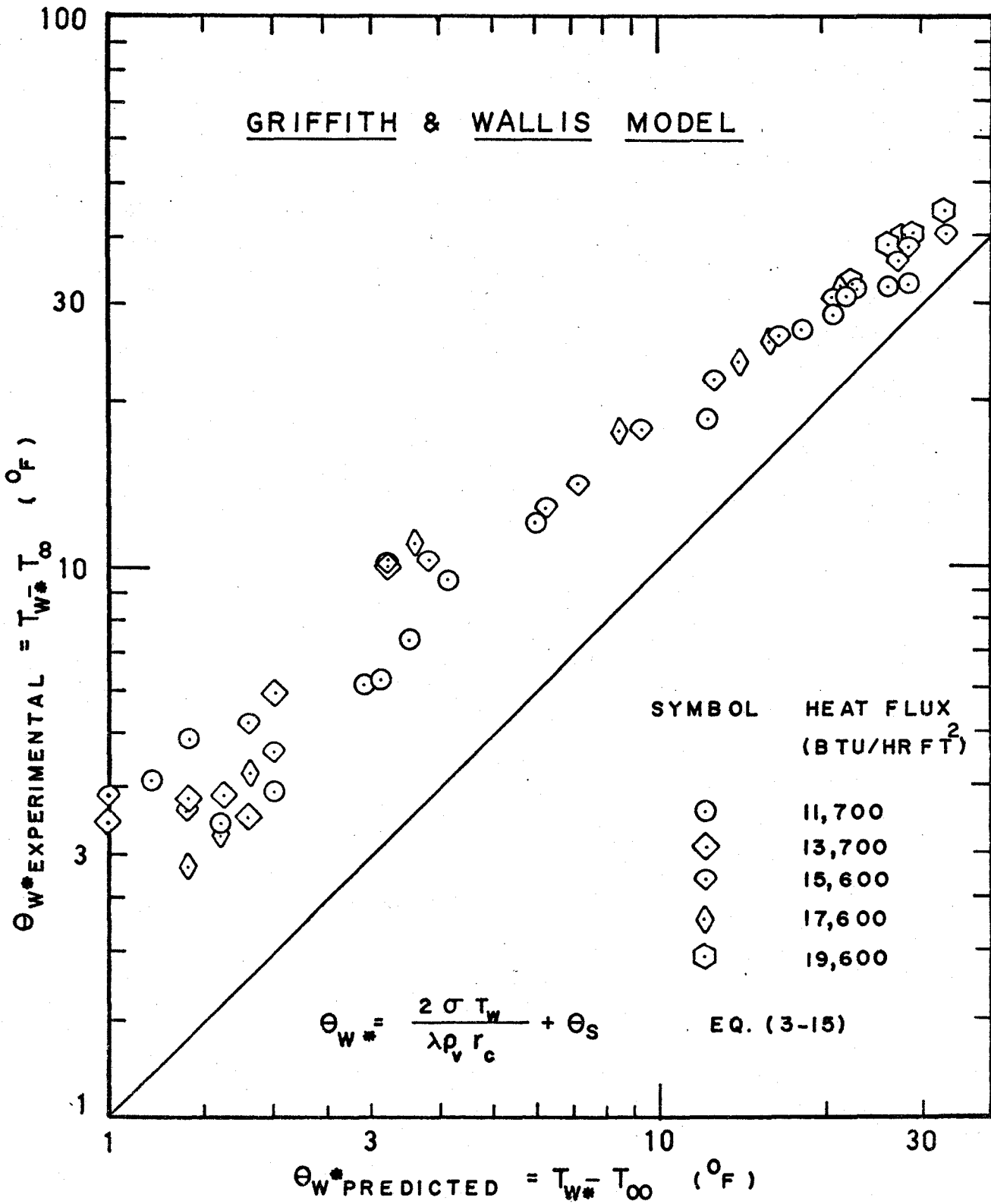


FIG. 18 $\Theta_{WE*} - \Theta_{WP*}$ CHARACTERISTICS

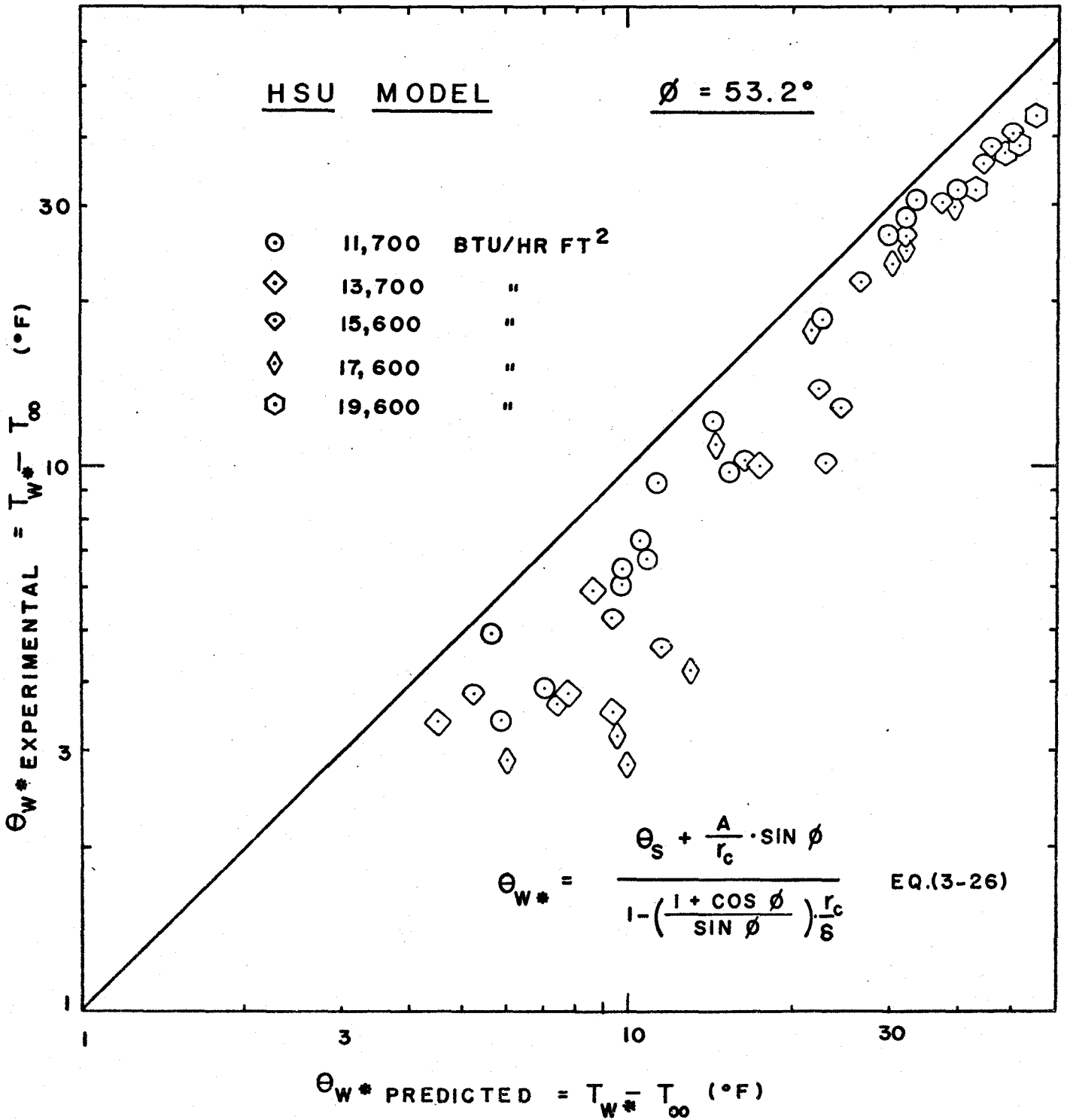


FIG. 19

$\Theta_{WE}^* - \Theta_{WP}^*$

CHARACTERISTICS

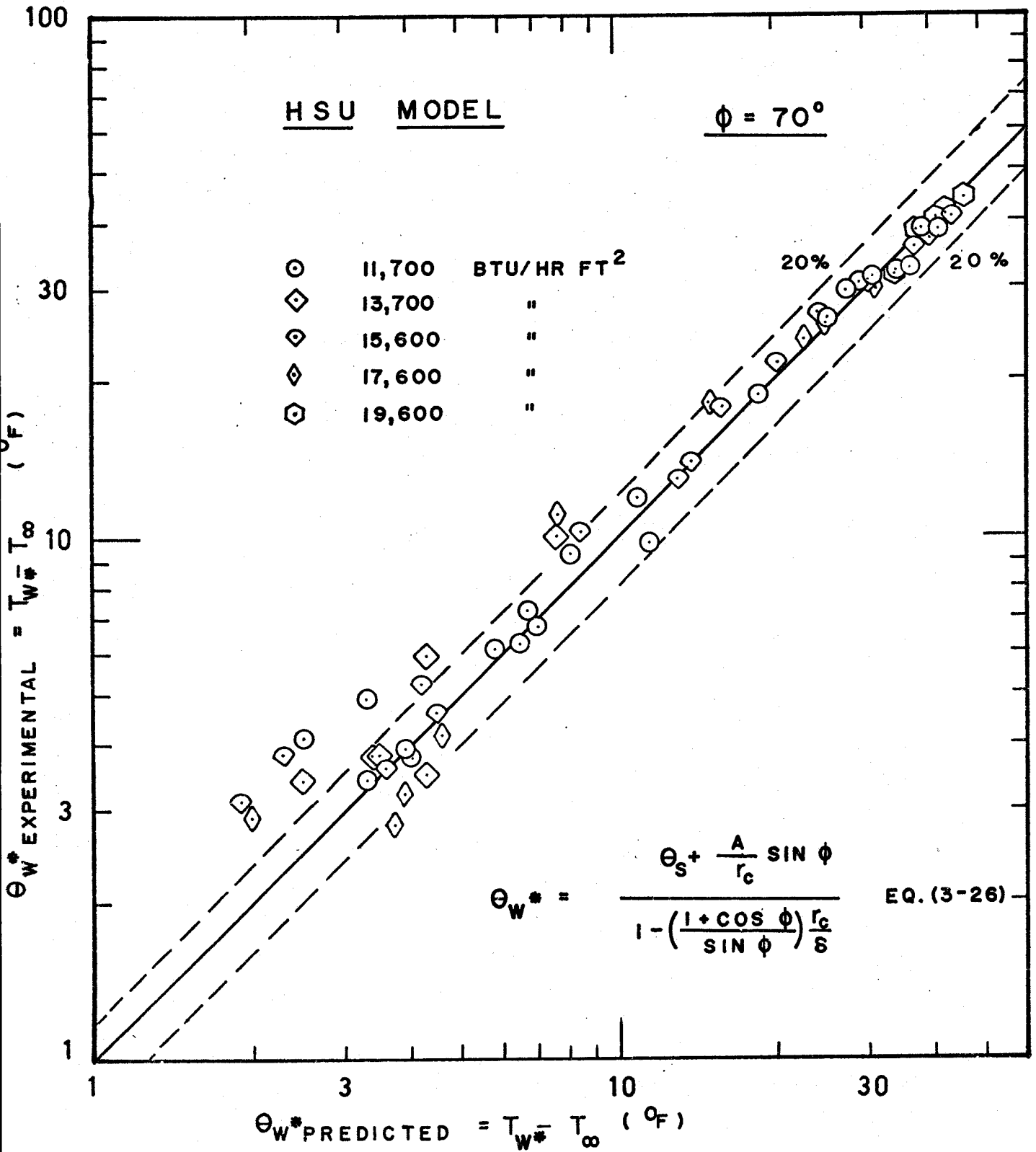


FIG. 20 $\Theta_{W^*}^{EXPERIMENTAL} - \Theta_{W^*}^{PREDICTED}$ CHARACTERISTICS

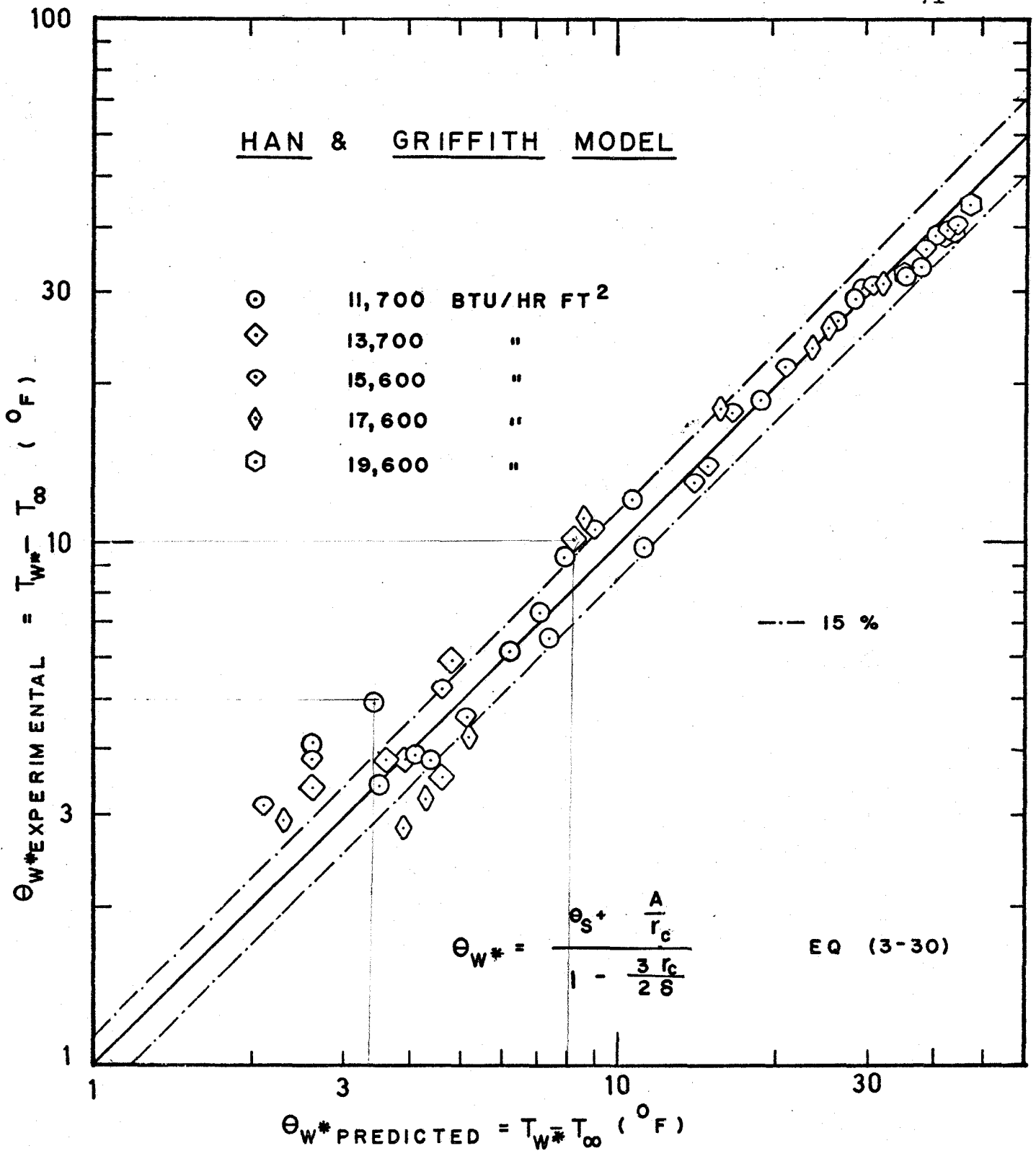


FIG. 21 $\Theta_{W^*}^E - \Theta_{W^*}^P$ CHARACTERISTICS

gives added support to the present investigation and at the same time demonstrates the validity of Hsu's model of bubble nucleation.

A still better agreement with experimental data is found in Han and Griffith's model, as shown in Figure 21. Moreover the expression for θ_{w*} is seen to be independent of contact angle ϕ . There is a great deal of uncertainty in measurement and selection of a value for the contact angle to be used in any particular experiment for bubble nucleation. Thus Han and Griffith's model proves superior to Hsu's model, in view of the present investigation in particular. Most of the experimental points lie within $\pm 15\%$ of the predicted value. The scatter is seen to be more toward the lower level of subcooling than that at the higher level. This is due to the fact that at lower subcooling the uncertainties in measurements of temperatures are higher than those at higher levels of subcooling.

CHAPTER IX

CONCLUSION

The investigation presents a set of measurements for water boiling at atmospheric pressure on a copper surface. Bubbles nucleating at an artificial site were observed for various heat fluxes. The measured initiation temperature differences show good agreement with the values predicted by Hsu, and Han and Griffith, thus enabling these models to be evaluated. Hsu's model was satisfactory but Han and Griffith's model was preferable inasmuch as it required no assumption for the contact angle. The present investigation also confirms Wiebe's superheat layer thickness measurements indirectly, since a satisfactory correlation for initiation temperature difference could not have been attained if these results were grossly in error.

A P P E N D I X A

EXPERIMENTAL DATA AND CALCULATIONS

The experimental data is presented here in tabular form and the predicted values for θ_{w*} are calculated using the mathematical models outlined in Chapter III. The equations governing θ_{w*} are reproduced here for convenience. Data for subcooling values within a range of $\pm 0.2^\circ\text{F}$ have been averaged and only the average values are shown in the following tables.

Griffith and Wallis:
$$\theta_{w*} = \frac{2\sigma T_w}{\lambda \rho_v r_c} + \theta_s$$

Hsu:
$$\theta_{w*} = \frac{\theta_s + \frac{A \sin\phi}{r_c}}{1 - \left(\frac{1+\cos\phi}{\sin\phi}\right) \frac{r_c}{\delta}}$$

Han and Griffith:
$$\theta_{w*} = \frac{\theta_s + \frac{A}{r_c}}{1 - \frac{3r_c}{2\delta}}$$

$T_{sa} - T_{\infty}$ $T_w - T_{\infty}$

TABLE III

q/A (BTU/Hr Ft ²)	θ_s (°F)	θ_w (°F)	θ_{wE}^* (°F)	h (BTU/Hr Ft ² °F)	δ (in. × 10 ³)	θ_{wP}^* (°F)			
						G&W	HSU		H&G
							$\phi=53.2^\circ$	$\phi=70^\circ$	
11,700	0.6	13.9	4.1	842	13.5	1.2	2.7	2.4	2.6
	0.8	12.6	4.9	930	10.8	1.4	5.6	3.1	3.4
	1.0	13.7	3.4	854	11.2	1.6	5.8	3.3	3.5
	1.2	12.9	3.9	908	10.9	1.8	7.1	3.9	4.1
	1.4	13.8	3.8	850	11.4	2.0	7.0	4.0	4.4
	2.3	14.5	6.1	806	11.7	2.9	9.7	5.8	6.2
	2.5	14.8	6.5	790	12.0	3.1	9.8	6.2	6.6
	2.9	15.4	7.3	762	12.3	3.5	10.5	6.7	7.1
	3.2	15.8	6.7	740	12.7	3.8	10.7	7.0	7.4
	3.5	16.5	9.3	709	13.0	4.1	11.1	7.8	7.9
	5.3	17.8	11.9	657	14.0	5.9	14.3	10.5	10.6
	5.8	18.2	9.7	644	14.3	6.4	15.1	10.8	11.2
	11.6	23.8	18.5	491	18.0	12.2	22.6	18.2	18.7
	17.5	28.4	26.3	408	21.0	18.1	29.9	25.2	25.8
	19.9	31.1	28.6	376	23.0	20.5	32.0	27.6	28.2

TABLE III - continued

q/A (BTU/Hr Ft ²)	θ_s (°F)	θ_w (°F)	θ_{wE}^* (°F)	h (BTU/Hr Ft ² °F)	δ (in. × 10 ³)	θ_{wP}^* (°F)			
						G&W	HSU		H&G
							$\phi=53.2^\circ$	$\phi=70^\circ$	
11,700	20.9	31.3	30.5	373	23.0	21.5	33.6	29.0	29.5
	21.9	32.7	30.7	358	23.5	22.5	34.8	30.1	30.4
	25.2	31.3	32.1	373	23.0	25.8	40.4	29.6	35.5
	27.1	39.3	32.5	295	28.0	27.7	39.3	34.8	38.1
13,700	0.4	13.8	3.4	994	10.3	1.0	4.5	2.5	2.6
	0.8	12.9	3.8	1060	10.0	1.4	7.7	3.5	3.6
	1.0	14.4	3.8	952	10.5	1.6	7.2	3.5	3.9
	1.2	13.4	3.5	1022	10.2	1.8	9.3	4.3	4.6
	1.4	14.8	5.9	925	10.7	2.0	8.6	4.3	4.8
	2.6	13.4	10.0	1022	10.2	3.2	17.2	7.6	8.2
15,600	0.4	14.7	3.8	1060	10.0	1.0	5.2	2.3	2.6
	0.8	15.1	3.6	1034	10.1	1.4	7.4	3.6	3.6
	1.2	15.2	5.2	1028	10.2	1.8	9.3	4.2	4.6

TABLE III - continued

q/A (BTU/Hr Ft ²)	θ_s (°F)	θ_w (°F)	θ_{wE}^* (°F)	h (BTU/Hr Ft ² °F)	δ (in. $\times 10^3$)	θ_{wP}^* (°F)			
						G&W	HSU		H&G
							$\phi=53.2^\circ$	$\phi=70^\circ$	
15,600	1.4	14.9	4.6	1048	10.0	2.0	11.5	4.5	5.1
	2.6	13.7	10.0	1138	9.7	3.2	22.7	8.2	9.0
	3.2	17.2	10.3	906	10.8	3.8	16.4	8.4	9.0
	5.6	20.1	12.7	776	11.2	6.2	24.2	13.2	14.1
	6.5	22.0	13.8	709	12.2	7.1	22.3	13.8	14.8
	8.6	23.9	17.4	652	14.2	9.2	22.1	15.8	16.4
	11.8	27.0	21.5	578	15.5	12.4	26.7	20.1	20.8
	15.9	30.1	26.1	518	17.2	16.5	31.9	25.2	26.0
	19.9	32.7	30.6	477	18.5	20.5	37.3	30.2	31.0
	26.3	37.8	35.6	412	21.0	26.9	44.6	37.5	38.4
	28.0	40.0	37.7	390	22.0	28.6	46.0	40.7	40.0
	28.2	40.6	37.0	384	22.5	28.8	45.7	39.2	39.9
	32.2	42.1	40.0	370	23.5	32.8	50.8	43.9	44.7
17,600	0.2	14.7	2.9	1198	9.4	0.8	6.0	2.0	2.3
	0.8	15.2	2.8	1158	9.6	1.4	9.9	3.7	3.9

TABLE III - continued

q/A (BTU/Hr Ft ²)	θ_s (°F)	θ_w (°F)	θ_{wE}^* (°F)	h (BTU/Hr Ft ² °F)	δ (in. $\times 10^3$)	θ_{wP}^* (°F)			
						G&W	HSU		H&G
							$\phi=53.2^\circ$	$\phi=70^\circ$	
17,600	1.0	16.3	3.2	1080	9.9	1.6	9.5	3.9	4.3
	1.2	15.3	4.2	1150	9.6	1.8	13.1	4.6	5.2
	3.0	19.5	11.1	902	11.0	3.6	14.5	7.7	8.3
	7.8	25.3	17.7	696	13.5	8.4	21.8	15.0	15.7
	13.6	30.3	23.6	580	15.7	14.2	30.2	22.8	23.6
	15.2	32.0	25.5	550	16.3	15.8	32.3	24.9	25.7
	20.1	34.8	30.6	505	17.7	20.7	39.1	31.2	32.1
19,500	21.4	37.1	32.2	528	17.0	22.0	43.2	33.9	34.9
	25.3	40.0	37.9	487	18.0	25.9	48.3	38.7	39.8
	27.0	41.8	38.2	470	18.7	27.6	49.8	40.5	41.5
	27.4	41.3	38.8	472	18.7	28.0	50.5	41.1	42.2
	28.1	41.3	39.4	472	18.7	28.7	51.8	42.1	43.2
	32.6	46.1	44.0	422	20.7	33.2	55.6	46.6	47.7

A P P E N D I X B

HEAT LOSS CALCULATION

Let us consider a control volume around the heating surface including the stainless steel skirt and the insulating plate, as shown in Figure 22. The heat transfer coefficients for the copper disc, the skirt and the insulating plate are h_b , h_c and h'_c respectively. The corresponding temperatures are T_W , T_S and T_P , and the ambient temperature is T_A .

Heat loss from the control volume to the surroundings takes place by convection and radiation.

L = length of the skirt = 2 inches

D = diameter of the skirt = 4 inches .

Taking the case of the minimum heat flow rate of $q = 300$ watts = 1025 BTU/Hr, the measured temperatures are

$$T_A = 75^\circ\text{F}$$

$$T_W = 221^\circ\text{F}$$

$$T_S = 175^\circ\text{F}$$

$$T_P = 120^\circ\text{F} .$$

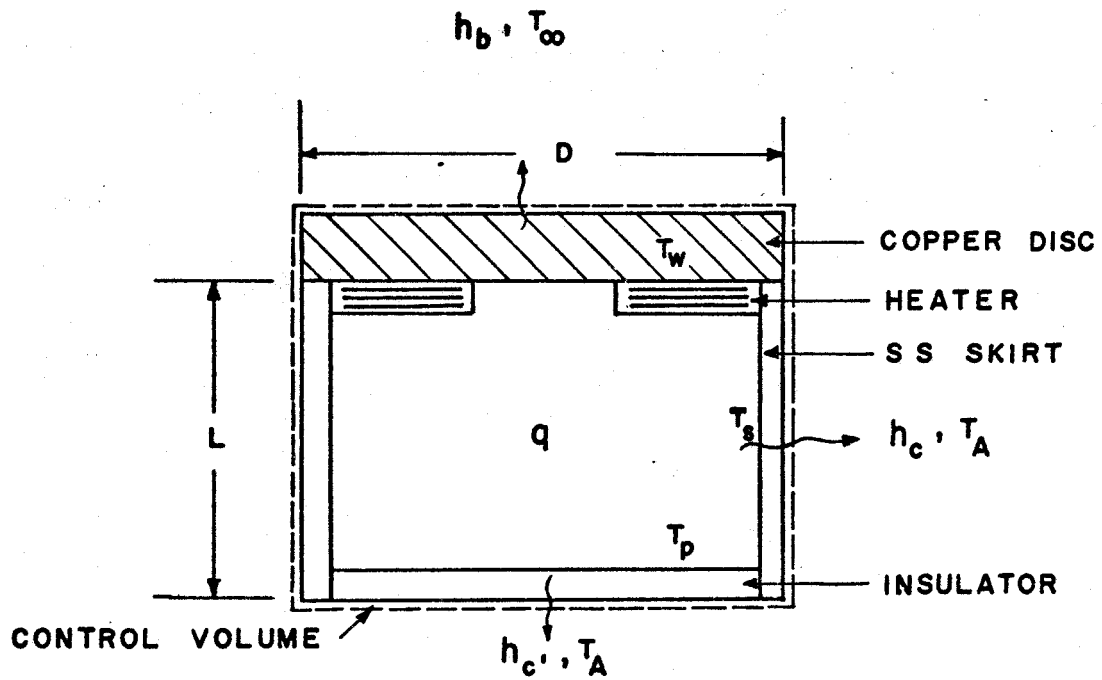


FIG. 22 HEAT LOSS CALCULATIONS

The heat transfer coefficients are defined [14] as

$$h_c = 0.29 \left(\frac{T_S - T_A}{L} \right)^{1/4} + \epsilon_S \sigma \left[\frac{T_S^4 - T_A^4}{T_S - T_A} \right]$$

$$h'_c = 0.12 \left(\frac{T_P - T_A}{D} \right)^{1/4} + \epsilon_P \sigma \left[\frac{T_P^4 - T_A^4}{T_P - T_A} \right] .$$

The total heat supplied by the heater can be accounted as consisting of three parts. The main part q' goes to heat the bulk liquid; one part is dissipated through the skirt to the ambient; and another part is lost through the insulating plate. Therefore,

$$q' = \frac{\pi}{4} D^2 h_b (T_w - T_\infty) \quad (B1)$$

$$q = \frac{\pi}{4} D^2 h_b (T_w - T_\infty) + \pi D L h_c (T_S - T_A) + \frac{\pi}{4} D^2 h'_c (T_P - T_A) \quad (B2)$$

and so

$$\frac{q'}{q} = 1 - \frac{\pi D L h_c}{q} (T_S - T_A) - \frac{\pi D^2 h'_c}{4q} (T_P - T_A)$$

$$= 1 - \frac{\pi D L}{q} \left[\frac{0.29 (T_S - T_A)^{5/4}}{L^{1/4}} + \epsilon_S \sigma (T_S^4 - T_A^4) \right]$$

$$- \frac{\pi D^2}{4q} \left[\frac{0.12 (T_P - T_A)^{5/4}}{D^{1/4}} + \epsilon_P \sigma (T_P^4 - T_A^4) \right] . \quad (B3)$$

From property table, suitable values of emissivities are chosen [14] as

$$\epsilon_s = 0.1$$

$$\epsilon_p = 0.6$$

$$\sigma = 0.1714 \times 10^{-8} \text{ BTU/Hr Ft}^2 \text{ } ^\circ\text{R}^4$$

= Stefan-Boltzmann constant

$$\begin{aligned} \frac{\pi DL}{q} & \left[\frac{0.29 (T_S - T_A)^{5/4}}{L^{1/4}} + \epsilon_s \sigma (T_S^4 - T_A^4) \right] \\ &= \frac{\pi \times 4 \times 2}{144 \times 1025} \left[\frac{0.29 (100)^{5/4}}{(2/12)^{1/4}} + 0.1 \times 0.1714 \times (6.35^4 - 5.35^4) \right] \\ &= 0.0268 \end{aligned}$$

and,

$$\begin{aligned} \frac{\pi D^2}{4q} & \left[\frac{0.12 (T_P - T_A)^{5/4}}{D^{1/4}} + \epsilon_p \sigma (T_P^4 - T_A^4) \right] \\ &= \frac{\pi (4/12)^2}{4 \times 1025} \left[\frac{0.12 (45)^{5/4}}{(4/12)^{1/4}} + 0.6 \times 0.1714 \times (5.80^4 - 5.35^4) \right] \\ &= 0.0043 \end{aligned}$$

Equation (B3) ultimately reduces to :

$$\frac{q'}{q} = 1 - 0.0268 - 0.0043 = 0.9689$$

$$\therefore \text{LOSS} = 1 - 0.9689 \approx 0.031 \quad .$$

Therefore, heat loss to the ambient is only 3.1 per cent of the total heat supplied by the heater.

A P P E N D I X C
UNCERTAINTY ANALYSIS

The uncertainty of each result computed was calculated using the following relationship

$$\frac{W_R}{R} = \left[\left(\frac{\partial R}{\partial V_1} \cdot \frac{W_1}{R} \right)^2 + \left(\frac{\partial R}{\partial V_2} \cdot \frac{W_2}{R} \right)^2 + \dots + \left(\frac{\partial R}{\partial V_n} \cdot \frac{W_n}{R} \right)^2 \right]^{1/2} \quad (C1)$$

where

R = result computed

W_R = uncertainty in the result R

V_n = nth variable

W_n = uncertainty in the nth variable .

Heat Flux:

$$\left(\frac{q}{A} \right)_{\text{actual}} = 11,700 \text{ BTU/Hr Ft}^2 \quad \text{at } q = 1024 \text{ BTU/Hr}$$

$$\left(\frac{q}{A} \right)_{\text{loss}} = 3.1\% = 362 \text{ BTU/Hr Ft}^2$$

$$h = \frac{q/A}{T_w - T_\infty}$$

$$\therefore \frac{W_h}{h} = \left[\left\{ \frac{\partial h}{\partial (q/A)} \cdot \frac{W_{q/A}}{h} \right\}^2 + \left\{ \frac{\partial h}{\partial (T_w - T_\infty)} \cdot \frac{W_{(T_w - T_\infty)}}{h} \right\}^2 \right]^{1/2} \quad (C2)$$

$$W_{(T_w - T_\infty)} = 0.5 + 0.5 = 1.0^\circ\text{F}$$

$$W_{q/A} = 362 \text{ BTU/Hr Ft}^2$$

$$h = 842 \text{ BTU/Hr Ft}^2 \text{ }^\circ\text{F}$$

$$T_w - T_\infty = 13.9^\circ\text{F}$$

$$\begin{aligned} \therefore \frac{W_h}{h} &= \left[\left\{ \frac{1}{13.9} \cdot \frac{362}{842} \right\}^2 + \left\{ -\frac{11,700}{(13.9)^2} \cdot \frac{1.0}{842} \right\}^2 \right]^{1/2} \\ &= 7.83 \times 10^{-2} \approx 7.8\% \end{aligned}$$

Superheat layer thickness:

$$W_\delta = \frac{0.0135 - 0.0127}{0.0135}, \text{ from Figure 17}$$

$$\approx 0.06$$

$$= 6\%$$

Initiation temperature difference θ_{w^*} :

$$\theta_{w^*} = \frac{\theta_s + \frac{A}{r_c}}{1 - \frac{3r_c}{2\delta}}$$

$$A = 2.3 \times 10^{-3} \text{ in.}^\circ\text{R} \quad \theta_s = 0.6^\circ\text{F}$$

$$\delta = 13.5 \times 10^{-3} \text{ in.} \quad \theta_{w^*} = 4.1^\circ\text{F}$$

$$r_c = 4.2 \times 10^{-3} \text{ in.}$$

$$\frac{\partial \theta_{w^*}}{\partial \theta_s} = \frac{1}{1 - \frac{3r_c}{2\delta}} = 1.88$$

$$\begin{aligned} \frac{\partial \theta_{w^*}}{\partial r_c} &= \left[\left(1 - \frac{3r_c}{2\delta}\right) \left(-\frac{A}{r_c^2}\right) - \left(\theta_s + \frac{A}{r_c}\right) \left(-\frac{3}{2\delta}\right) \right] / \left[1 - \frac{3r_c}{2\delta}\right]^2 \\ &= 0.20 \times 10^3 \end{aligned}$$

$$\begin{aligned} \frac{\partial \theta_{w^*}}{\partial \delta} &= - \left(\theta_s + \frac{A}{r_c}\right) \left(\frac{3r_c}{2\delta^2}\right) / \left(1 - \frac{3r_c}{2\delta}\right)^2 \\ &= - 0.14 \times 10^3 \end{aligned}$$

$$\begin{aligned} \therefore \frac{W_{\theta_{w^*}}}{\theta_{w^*}} &= \left[\left(\frac{\partial \theta_{w^*}}{\partial \theta_s} \cdot \frac{W_{\theta_s}}{\theta_{w^*}}\right)^2 + \left(\frac{\partial \theta_{w^*}}{\partial r_c} \cdot \frac{W_{r_c}}{\theta_{w^*}}\right)^2 + \left(\frac{\partial \theta_{w^*}}{\partial \delta} \cdot \frac{W_{\delta}}{\theta_{w^*}}\right)^2 \right]^{1/2} \\ &= \left[\left(1.88 \times \frac{0.6}{4.1}\right)^2 + \left(0.20 \times 10^3 \times \frac{0.5 \times 10^{-3}}{4.1}\right)^2 \right. \\ &\quad \left. + \left(-\frac{0.14 \times 10^3 \times 0.81 \times 10^{-3}}{4.1}\right)^2 \right]^{1/2} \\ &= [0.0757 + 0.0006 + 0.0008]^{1/2} \\ &= [0.0771]^{1/2} = 0.277 = 27.7\% \quad (C4) \end{aligned}$$

Therefore, the uncertainties are:

Heat flux $\frac{q}{A}$ (11,700 BTU/Hr Ft ²)	3.1%
Heat transfer coefficient h (842 BTU/Hr Ft ² °F)	7.8%
Superheat layer thickness δ (13.5 × 10 ⁻³ inches)	6.0%
Initiation temperature difference θ_{w*} (4.1 °F)	27.7%

REFERENCES

1. Corty, Claude and Foust, A. S., "Surface Variables in Nucleate Boiling", Chem. Eng. Prog. Sym. Series, No. 17, Vol. 51, 1955.
2. Bankoff, S. G., "The Prediction of Surface Temperatures at Incipient Boiling", Chem. Eng. Prog. Sym. Series, No. 29, Vol. 55, 1957.
3. Griffith, P. and Wallis, J. D., "The Role of Surface Conditions in Nucleate Boiling", ASME-AIChE Heat Transfer Conf., Storrs, Conn., 1959.
4. Hsu, Y. Y., "On the Range of Active Nucleation Cavities on a Heating Surface", Trans. ASME, August 1962.
5. McAdams, W. H., Addams, J. N. and Kennel, W. E., "Heat Transfer at High Rate to Water with Surface Boiling", Dept. Chem. Eng., M.I.T., December 1948.
6. Han, C. and Griffith, P., "The Mechanism of Heat Transfer in Nucleate Pool Boiling", Int. J. Heat Mass Transfer, Vol. 8, 1965.
7. Judd, R. L., "Influence of Acceleration on Subcooled Nucleate Boiling", Ph.D. Thesis, University of Michigan, Univ. Microfilms Inc. #69-12148.

8. Wiebe, J. R. and Judd, R. L., "Superheat Layer Thickness Measurements in Saturated and Subcooled Nucleate Boiling", J. Heat Transfer, November 1971.
9. Fishenden, M. and Saunders, O. A., "An Introduction to Heat Transfer", Oxford, 1960.
10. Lippert, T. E. and Dougall, R. S., "A Study of the Temperature Profiles Measured in the Thermal Sublayer of Water, Freon 113, and Methyl Alcohol During Pool Boiling", J. Heat Transfer, No. 3, Vol. 90, August 1968.
11. Bobst, R. W. and Colver, C. P., "Temperature Profiles up to Burnout Adjacent to a Horizontal Heating Surface in Nucleate Pool Boiling Water", Chem. Eng. Prog. Sym., No. 82, Vol. 64, 1968.
12. Judd, R. L. and Merte, H., Jr., "Influence of Acceleration on Subcooled Nucleate Pool Boiling", Fourth Int. Heat Transfer Conf., Paris-Versailles, 1970.
13. Rao, S. N., "Effect of Surface Active Agents in Boiling Heat Transfer", M. Eng. Thesis, McMaster Univ., 1967.
14. McAdams, W. H., "Heat Transmission", 3rd.ed., McGraw-Hill Book Company, New York, 1954.

NOMENCLATURE

SYMBOLS	DESCRIPTIONS	UNITS
A	Parameter $A = 2\sigma T_s / \lambda \rho_v$	Ft °R
C_1	Constant $C_1 = (1 + \cos\phi) / \sin\phi$	-
C_2	Constant $C_2 = 1 / \sin\phi$	-
C_3	Constant $C_3 = (1 + \cos\phi)$	-
c	Specific heat	BTU/lbm °F
f	Frequency of bubble emission	1/sec
J	Mechanical equivalent of heat	Ft lbf/BTU
h	Heat transfer coefficient	BTU/Hr Ft ² °F
k	Thermal conductivity	BTU/Hr Ft °F
N/A	Active site density	1/in ²
Nu	Nusselt number	-
Pr	Prandtl number	-
Gr	Grashof number	-
q/A	Heat flux	BTU/Hr Ft ²
T	Time average temperature	°R
P	Pressure	lbf/Ft ²
V	Velocity	Ft/sec
r	Radius of cavity mouth	in.
b	Bubble height	in.
δ	Extrapolated superheat layer thickness	in.
θ	Temperature difference $\theta = T - T_\infty$	°F
ϕ	Contact angle	-

NOMENCLATURE - continued

SYMBOLS	DESCRIPTIONS	UNITS
λ	Latent heat of vaporization	BTU/lbm
ρ	Density	lbm/Ft ³
σ	Surface tension	lbf/Ft
μ	Coefficient of viscosity	lbm/Hr Ft
α	Thermal diffusivity	Ft ² /Hr

SUBSCRIPTS	DESCRIPTION
l	liquid
v	vapor
w	surface
∞	bulk
s	saturation
o	incipience
w*	center line
E	experimental
P	predicted
i	interface
n	nucleus
b	bubble